CHAPTER 6

Thermal Energy Storage Design of a New Bifacial PV/PCM System for Enhanced Thermo-electric Performance

In this chapter, a new concept of bifacial PV/PCM (BIF-PV/PCM) system with sandwiched thermal energy storage enclosure has been investigated that possesses 1.21 times power output density and 7.39 times total energy utilization density per unit land area compared to the conventional PV system. Based on the melting morphology and thermo-electric performance of the initially rectangular PCM enclosure, an optimized bifurcated non-rectangular design of the enclosure is proposed to enhance the incident radiation utilization ability by 87% more than a simple one PV/PCM system. Enhanced utilization of solar radiation manifests into 105% more melting compared to conventional PV/PCM system. With the strategic mirror reflection and bypassing the solar radiation towards the rear PV panel and strategic design of PCM enclosure to aid convection-driven melting, electric power output has been increased significantly (about 77%) compared to similar conventional PV/PCM system. The study revealed that overall system efficiency could approach about 74% if suitable strategies are adopted, as demonstrated in this chapter. Results are discussed in terms of energy utilization efficiency, exergy efficiency, power conversion efficiency, tracking melting front morphology, and its effect on heat transfer characteristics, etc. This investigation has been carried out with the help of an experimentally validated numerical model that accurately mimics the melting morphology of PCM and other heat transfer characteristics of the system. The findings of this study would help design and develop a more efficient BIF-PV/PCM system to meet exponentially increasing energy needs.

6.1 Introduction

Energy transformation heavily relies on reducing energy-related CO_2 emissions. Sooner the world shifts from fossil fuels better would be the chance to achieve climate goals [2, 79]. Photovoltaic (PV) technology is a promising and growing option to produce pollution-free and clean energy by harnessing solar energy to meet global energy demands [5, 83]. PV technology is becoming the preferred choice to generate electricity across the globe. This can be judged from the fact that about 120 GW of new solar PV projects were installed in the year 2020 alone [90]. Large scale and accelerated deployment of PV technology will be required combined with increased energy efficiency if Paris climate goals are met by 2050. A quarter (25%) of the world's electricity will be generated by solar PV by 2050 [13]. However, in the long run, several barriers and constraints still need to be overcome.

The primary constraints for large-scale deployment of PV modules are lower power output density (power output per unit land area) and operational efficiency. PV technology relies on low energy density solar radiation; hence, ample open space must intercept the incoming radiation [91]. And with land acquisition coming at a considerable premium, the future proliferation of PV technology might face challenges. On the other hand, its low electrical efficiency (about 10-16%) is another significant drawback compared to other renewable energy sources (e.g., hydropower plant efficiency is 90%, wind turbine efficiency is 60%) [11, 76]. Since PV technology is slowly becoming mature, wringing additional costs and enhancing efficiency out of solar energy has become scientifically challenging [92]. Recently, it was suggested to develop bifacial modules, which can capture photons that are reflected off the ground to the backside of panels. This might increase electric power efficacy by 5–10% [93–95]. On the face of it, theoretically, the bifacial PV technology looks promising as it would reduce the land requirement and increase electricity production to some extent [96, 97]. Both the constraints discussed above seem to be overcome by bifacial technology. However, there is a considerable thermal limitation.

It is a well-known fact that a PV module rejects a significant amount of heat due to lower electric conversion efficiency. The wasted heat further deteriorates the electric performance of the PV panel by increasing its temperature [36, 40, 98]. Hussain et al. [10] reported a declination rate of 0.5%/°C rise of crystalline (c-Si) PV cell temperature. In the case of a bifacial PV module, where electricity is generated from both sides, a significant temperature rise may further deteriorate its electrical performance [99, 100]. Hence, to make this bifacial technology viable, further the research on thermal management (controlling PV cell temperature) and insolation management (managing the incoming radiation) for a given land area is needed. Thermal management strategies such as photovoltaic thermal (PV/T) systems [44, 47, 84, 85, 101], photovoltaic thermal systems integrated with phase change material (PV/T-PCM) [54, 102**?**], photovoltaic systems integrated with phase change material (PV/PCM) [66, 86, 103, 104] have been reported to improve the electrical performance of PV panels.

PV/PCM systems have become center of attraction among researchers due to its high heat storing capacity of phase change material (PCM) and use of this stored heat during nocturnal hours for various applications [50, 52, 58, 59]. Nada et al. [58] reported a reduction of 8.1°C in PV cell temperature with use of PCM enclosure only which enhances its electric conversion performance by 5.7%. In an experimental study, Li et al. [59] observed an increment of 5.18% in electrical performance of PV panel due to substantial temperature reduction (23°C) for PV/PCM system. Further, Kibria et al. [52] exhibit an enhancement of 5% in electric conversion performance by adopting PCM enclosure as waste heat storing device. Lu et al. [50] reported a reduction of 20°C in PV panel temperature and 10% enhancement in electrical performance. Therefore, it can be concluded from the literature that use of PCM enclosure is a viable thermal management strategy for PV panels. PCM enclosure helps in maintaining PV panels at low operating temperature without any extra consumption of power. In PV/PCM systems, the PCM enclosure is exposed to one side heating while two side heating will be observed in bifacial PV/PCM systems. Therefore, to the author's knowledge, a detailed study on the thermal energy storage design of a bifacial PV/PCM system is yet to be conducted in detail.

Figure 6.1 shows the basic mono-facial PV panel integrated with a rectangular PCM enclosure. Heat rejected from the PV module is stored in the PCM at a constant lower temperature during the phase change, thus helping the module operate in proximity of melting temperature of PCM. Figure 6.2 shows proposed initial design of a bifacial PV/PCM system incorporating both thermal and insolation management strategies. The high storage capacity and ability of PCM to store heat make it a suitable option for the thermal management of bifacial PV systems. PCM is sandwiched between two PV panels to create a bifacial PV/PCM (BIF-PV/PCM) system. BIF-PV/PCM system consists of PV panel on both front and rear side of the PCM enclosure and bypassed solar radiation is incident on the backside by reflecting with L-shape mirror system. This arrangement will be advantageous due to its high electric power output efficacy (additional 20-30% higher electrical output if solar tracking is used) as well as high thermal storage. However, the shape and size of such a storage system that is best suited for a bifacial PV system are unknown and scientific literature is scarce on its thermo-electrical performance. The additional advantage of these BIF-PV/PCM systems is that they can reduce the cooling load of a building when integrated with roof or walls as most of the incoming radiation is reflected back to surroundings.

It is to be noted that non-uniform PV temperature is not the desired criteria as it affects the efficiency and durability of the panel in the long run. A uniform PV panel temperature can be achieved if the melting morphology of the PCM aid the convection-dominated melting regime than conduction melting [39]. Since heat generation occurs from both sides in the bifacial system, buoyancy forces are expected to make the melting morphology complex [105]. Hence, various design concepts of thermal storage enclosure have been carried out in this study to arrive at an efficient enclosure design that significantly enhances the thermo-electrical performance

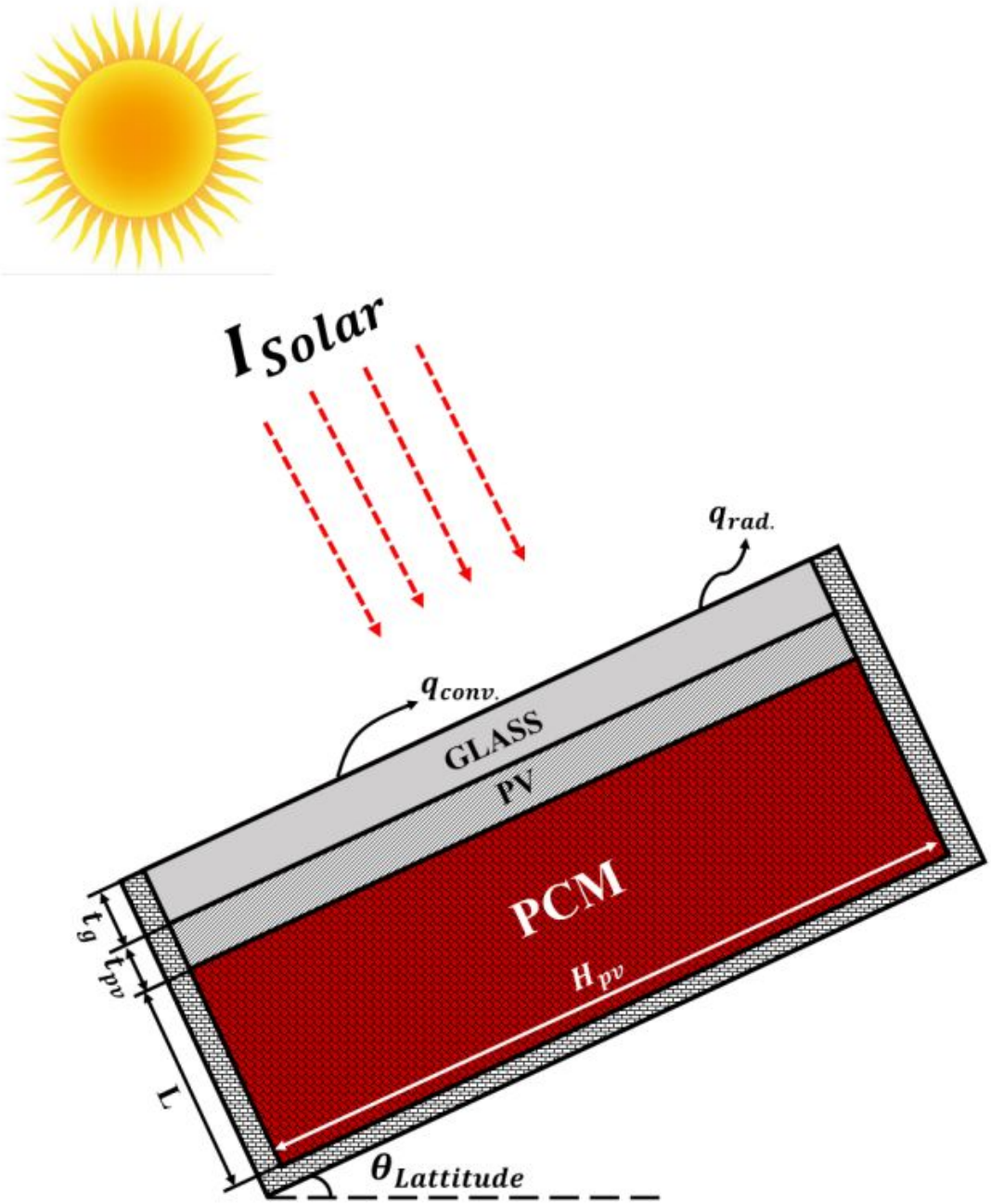

Figure 6.1: Schematic diagram of conventional PV/PCM system.

of the system.

The primary objective of the study is three-fold: First, to enhance the thermo-electric performance by managing the incoming radiation (insolation management) for a given atmospheric condition and volume of PCM enclosure. This objective is achieved by using two PV panels and reflecting the radiation to the rear PV panel. Such design configuration is expected to produce increased power and heat energy per unit land area. Second, to maximize the thermo-electric performance by controlling the PV panel temperature (thermal management). This objective is achieved by optimizing the PCM enclosure design to improve the duration of the quasi-

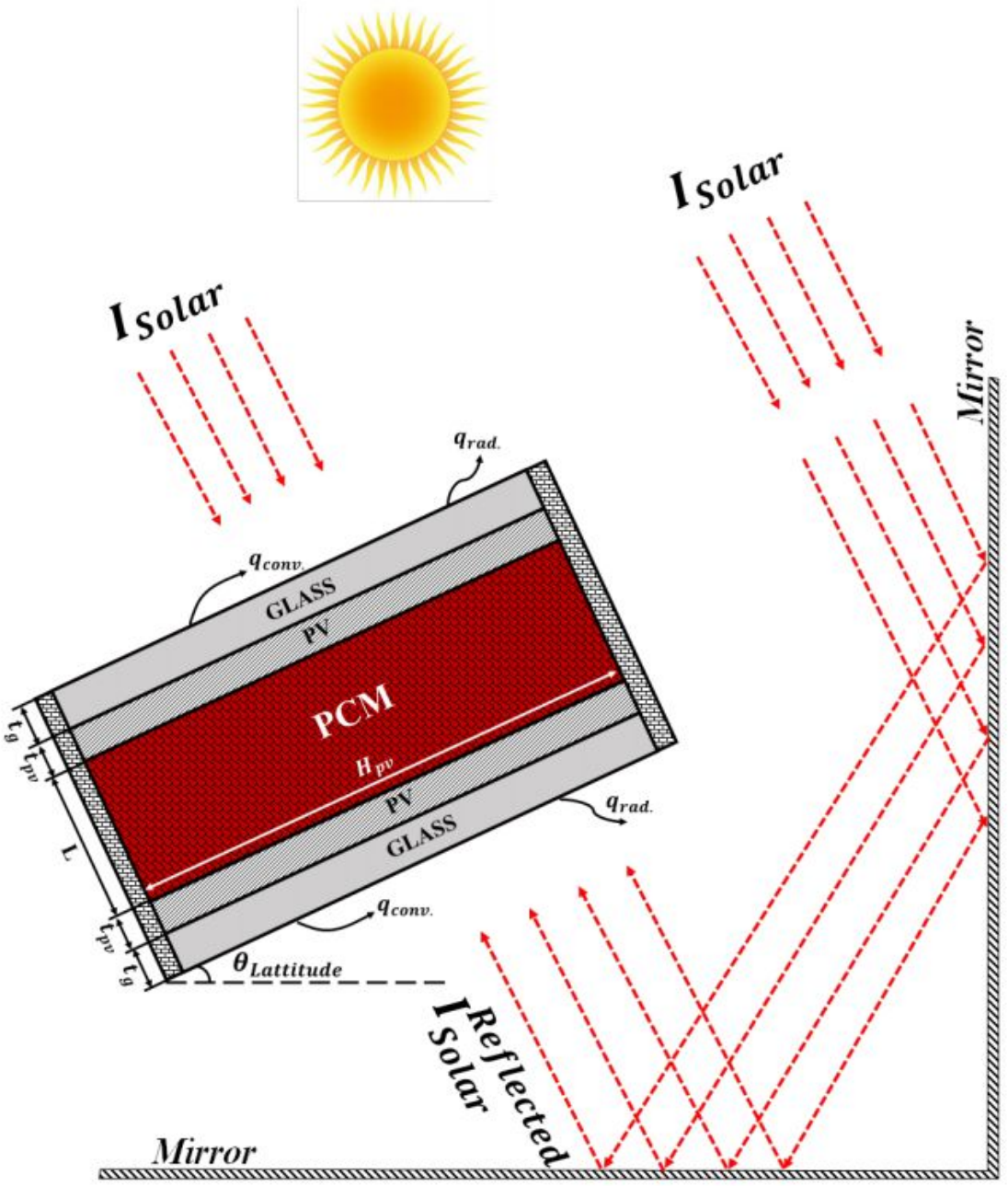

Figure 6.2: Schematic diagram of BIF-PV/PCM system with sandwiched rectangular PCM unit.

convection regime (delaying interaction of two melting fronts in this case). Usually, rectangular PCM enclosure designs have been studied when a single inclined PV panel is used [51, 106]. It is expected that melting characteristics of sandwiched PCM would be different when two PV panels are used. With changing melting morphology, PCM enclosure design becomes different [39]. Hence, the third objective is to characterize the melting morphology of the new designs, and analyze its effect on electric and thermal storage performance of the systems. A comparative investigation of the thermo-electric performance of different configurations of BIF-PV/PCM systems and PV/PCM systems has been performed under same boundary conditions using an

experimentally calibrated numerical model. The influence of reflecting radiation and enclosure shape on PCM melting rate on thermo-electric performance of BIF-PV/PCM system has been investigated and compared to simple PV/PCM system. Such nature of investigations in a bifacial PV panel sandwiching PCM system is rare in scientific literature.

6.2 Solution methodology

6.2.1 Problem formulation

Figure 6.1 depicts the schematic diagram of the PV/PCM system, which consists of a glass region of a thickness(t_g), a PV region of a thickness (t_{pv}), and a PCM region of the rectangular shape of a thickness (L) with a height of PV panel(H_{pv}). The PV/PCM system is inclined on the latitude angle to ensure the normal radiation to the system. Solar radiation (I_{solar}) is incident on the glass layer and transmitted to PV panel, which converts some part of it to electric power and rest of it is transferred as waste heat to PCM enclosure where it is stored as latent heat in the PCM. Figure 6.2 shows the schematic diagram of sandwiched BIF-PV/PCM system, which consists of additional layer of the PV panel and glass on the back of PV panel. In BIF-PV/PCM system, the solar radiation above and around the system is reflected back to the PV panel on the rear side of the system. This additional reflected incident radiation ($I_{solar}^{reflected}$) manifests into additional electric power output and additional stored energy as well. Figure 6.3 shows the improved BIF-PV/PCM system after the observing the results from system shown in Figure 6.2. The PCM enclosure is modified into bifurcated type non-rectangular enclosure (combined PCM volume remains same as of rectangular enclosure). RT27 is chosen as PCM, and thermo-physical properties of all materials used in different regions of the system are listed in Table 2.2. Glass and PV materials are treated as solid. In contrast, PCM material is modeled as a multiphase region that can change phase by absorbing or releasing heat energy. Initially, PCM is solid and governed by conductive heat transfer and gets melted to liquid on reaching the phase transition temperature. Liquid PCM is also governed by the conduction mode of heat transfer initially, but later it is purely dominated by the natural convection mode of heat transfer. All the thermo-physical properties of PCM are considered homogenous and invariable except density which varies with temperature according to Boussinesq approximation in the liquid phase of the material.

6.2.2 Boundary conditions

Solar radiation (I_{solar}) incident normally on the top wall of the glass layer where some part of it is lost to surroundings in form of convective and radiative heat flux losses. The remaining radiation is conducted into the wall to PV panel and then PCM enclosure. Hence, energy balance at the top wall can be given as:

$$I_{solar} = q''_{in} + q''_{loss} \tag{6.1}$$

where, q''_{in} denotes the conductive heat transfer into the system and q''_{loss} is the cumulative effect of convective heat loss (q''_{conv}) and radiative heat loss (q''_{rad}) to the ambient, which can be written as:

$$q''_{in} = |-kdT/dx|, \tag{6.2}$$

$$q''_{loss} = h_t(T_s - T_a), \tag{6.3}$$

In Eq. 6.3, T_s denotes the surface temperature of the top wall and $T_a$represents the ambient temperature and h_t is cumulative heat transfer coefficient provided to the top wall to count the radiative and convective losses to the surrounding from the system. Hence,

$$h_t = 5.7 + 3.8v_w \tag{6.4}$$

The cumulative heat transfer coefficient is calculated by Eq. 6.4 as suggested by Singh and Singh [107] where, v_w is the velocity of wind in m/s.

In PV/PCM system (Figure 6.1), all other boundaries are kept perfectly insulated. In contrast, reflected solar radiation ($I^{reflected}_{solar}$) is incident on the bottom surface of the system in addition to the incident solar radiation on the top surface of the system in the BIF-PV/PCM system (Figure 6.2 and 6.3). Energy balance on the bottom surface of BIF-PV/PCM system can be written as:

$$I^{reflected}_{solar} = q''_{in} + q''_{loss} \tag{6.5}$$

Conductive heat transfer into the system(q''_{in}) through bottom wall can also be calculated using Eq. 6.2. The heat loss to the surroundings from the system for bottom wall can be calculated by the relation given in Eq. 6.4. In BIF-PV/PCM system, all other boundaries except the top and bottom walls are kept perfectly insulated.

In the current study, various numerical simulations have been conducted for comparison of thermoelectric performance of PV/PCM system (Figure 6.1), BIF-PV/PCM system (Figure 6.2), and modified BIF-PV/PCM system (Figure 6.3). The nearby radiation is reflected with the help of reflecting mirrors to the backside of the BIF-PV/PCM system to increase the yield of electric power and thermal energy storage. The ratio (V_L/V_R) for modified BIF-PV/PCM system depends on the ratio of incident radiation on top PV panel to reflected radiation on bottom PV panel and orientation of PV panel. The ratio (V_L/V_R) is the ratio of volume of PCM in left side of enclosure (attached to top PV panel) to volume of PCM in right side of enclosure (at-

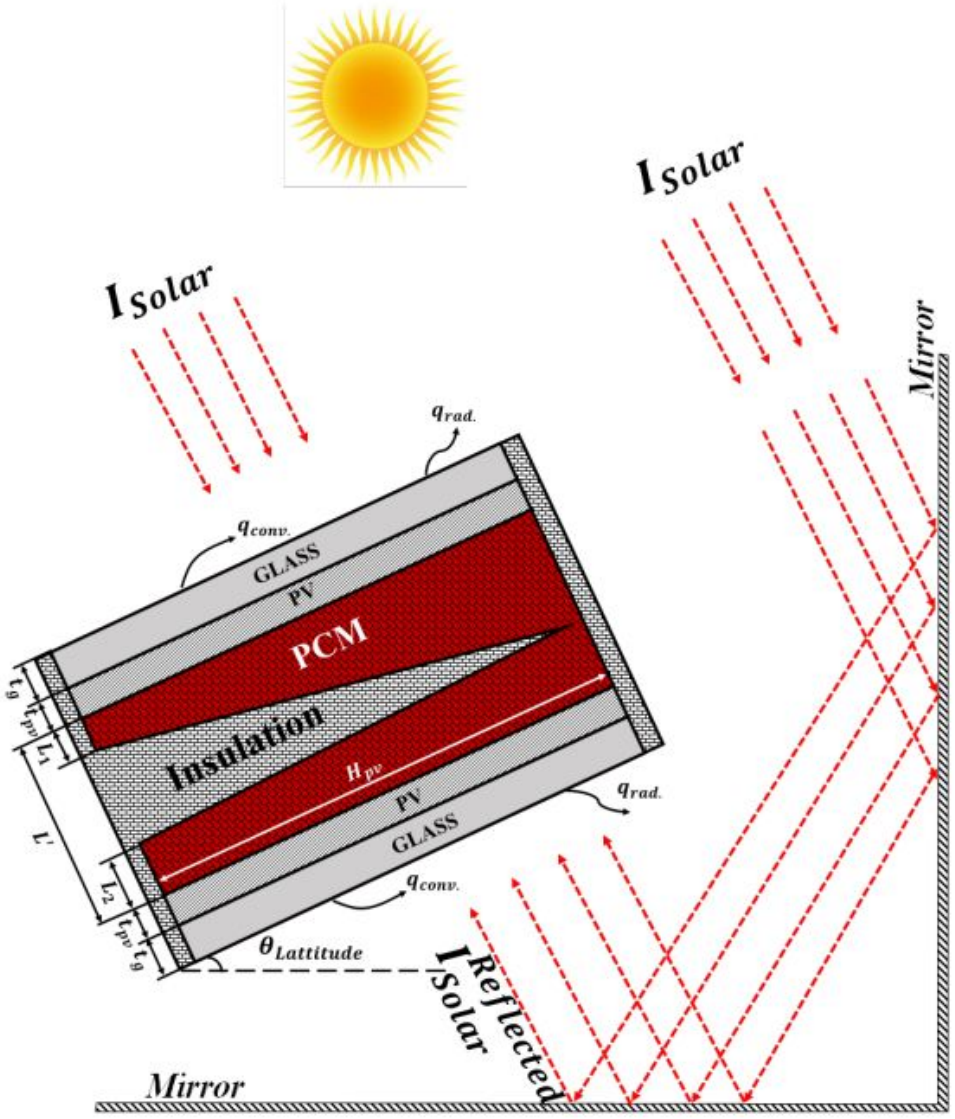

Figure 6.3: Schematic diagram of modified BIF-PV/PCM system. Note how the rectangular PCM enclosure is modified to a bifurcated non-rectangular design. This design has been arrived after studying the melting front in the rectangular design.

tached to bottom PV panel). This ratio depicts the distribution of PCM for each PV panel as incident radiation would be different for both panels, and melting pattern in right enclosure is different due to bottom-side heating. The BIF-PV/PCM system is assumed to be inclined at an angle of 25° (approx. latitude of Varanasi, India) for normal incident radiation. Constant solar radiation ($I_{solar} = 800 W/m^2$) is considered to incident on top PV panel while reflected solar radiation $I_{solar}^{reflected} = (\gamma\varepsilon)_{m1}(\gamma\varepsilon)_{m2} I_{solar}$ is considered lower for bottom PV panel. The factor $\gamma\varepsilon$ is the product of reflectivity and emissivity for mirror m_1 and m_2, respectively. The silver coating is used to reflect approx. 99.9% of radiation while the glass of the mirror exhibits an emissivity (0.85-0.9). The incident radiation is considered constant because solar radiation during peak hours (11 AM to 1 PM) is nearly constant, and the heating issues of PV

panels are more severe during this period. The reduced radiation is due to absorption of some radiation by reflecting mirror and various other losses. Hence, optimum V_L/V_R = 16/14 is selected based on various simulations on the criterion of maximum (96.53%) and uniform melting than other configurations(V_L/V_R = 18/12, V_L/V_R = 17/13, $and V_L/V_R$ = 15/15 exhibits 92.10%, 94.11%, and 94.23% melting, respectively). The ambient temperature (T_a) and wind speed (v_w) are taken 20°C and 2.4 m/s, respectively.

6.2.3 Numerical solution

The conservation equations and other governing equation used for current investigations are shown by Eqs.2.7-2.14. To discretize and solve conservation equations and other governing equations, the same assumptions and solution methodology as in section 2.2.2 (solution method) of chapter 2 are utilised. L_{20} PV/PCM system (PV/PCM system with PCM enclosure thickness, L = 20 mm) is considered for grid-independent and time-independent study. After various analyses, a time step of 0.05s was found suitable for the study. Four different numbers of grids 100 × 29, 133 × 41, 200 × 53, and 267 × 65 are considered for grid-independent analysis and 200 × 53 was found suitable numbers of grids for the system. Properties like temperature, liquid fraction shows negligible variation beyond this grid size. Convergence is obtained by minimizing the relative error in inner iterations and by establishing the conservation of energy..

6.2.4 Experimental calibration of numerical model

The heat transfer mechanism in the glass and PV layers is dominated by conduction only, while the PCM region exhibits a bit complex mechanism of heat transfer (different regimes). Therefore, the current numerical model for conventional PV/PCM system is calibrated by reproducing the experimental findings of Kamkari et al. [37] on natural convection-driven melting within a rectangular enclosure. We also calibrated our numerical model with the experiments of Fadl and Eames [39] who presented two side PCM heating and melting characteristics as in our model. In Kamakari's [37] investigation, the melting behavior of PCM (Lauric acid) is analyzed by applying constant temperature (70°C) at one vertical wall of the rectangular enclosure and keeping other walls perfectly insulated. The liquid fraction is plotted against time (Figure 6.4(a)) to compare numerical observations with experimental data. It can be observed that the numerical curve shows a close similarity with the experimental measurements curve. The numerical model took the approximately equal time (196 minutes) for complete melting of PCM, which is of the same order of magnitude as reported experimentally (198.5 minutes). Moreover, solid-liquid interface patterns are also compared at specific times, and both of the models exhibit similar melting patterns.

In Fadl and Eames [105] study, the melting behavior of PCM (RT44HC) is analyzed by applying uniform heat flux on both vertical walls of the rectangular enclosure. Liquid fraction –

time curve is compared for experimental and numerical findings in Figure 6.4(b). The curve for numerical study follows the experimental data closely. The melting time of PCM in the numerical model (308.6 minutes) is approximately equal to experimental findings (315.7 minutes). The comparison of melting front contours at specific times also exhibits similar trends. The numerical model shows some marginal deviation compared to the experimental model because of the following reason: (i) PCM in the numerical model is assumed to have constant phase transition temperature, however lauric acid and RT44HC both exhibit mushy zone of some range of temperature, (ii) same and invariable thermo-physical properties of PCM is assumed for both the phases in the numerical model which is not valid for either of PCMs, (iii) uncertainty in experiments, (iv) numerical error. Hence, the numerical model is presumed to capture the physics involved in the experimental setup.

6.3 Results and discussions

6.3.1 Solid-liquid interface patterns

Figure 6.5 highlights the transient melting history of PCM in PV/PCM systems and BIF-PV/PCM systems. The heat transfer and melting mechanism can be adequately understood by tracking the motion of the solid-liquid interface within the enclosure. The absorbed radiation from the PV panel is transmitted to the PCM enclosure in the form of waste heat, which channelizes a gravity-driven flow of liquid PCM in the enclosure with time. Hence, storing of heat by PCM strongly depends on modes of heat transfer within the PCM enclosure. Initially, melting is governed by conduction only because viscous forces dominate in the liquid PCM region. With the progression of melting, gravity-driven buoyancy force overcomes the viscous forces, and convective melting is observed in the top part of the enclosure, while at the bottom, conduction still dominates. Hence, melting is governed by mixed (convection and conduction) mode of heat transfer. With time, buoyant forces developed in all melted region of the enclosure, and melting is governed by the convective mode of heat transfer. The melting process in this fully developed convective mode of heat transfer is also called the quasi-steady convection regime of melting, which ends as the melting front reaches the bottom wall. The strength of convection current starts to decline, and the solid starts to shrink to the lower region of the enclosure. This regime of melting is called the solid-shrinking regime of melting.

Figure 6.5(a) shows the melting process for PV/PCM system with enclosure thickness(L_{20}). It can be easily visualized that the conduction regime of melting extends approximately up to 15 minutes. The melting interface is parallel to the PV panel in this regime of melting. With the development of convection current in the upper region of the enclosure, the melting interface gets eroded, and this erosion is visible at 30 minutes of the process. The melting interface is parallel to the PV panel in the lower region, but in the upper region, it loses its symmetry due

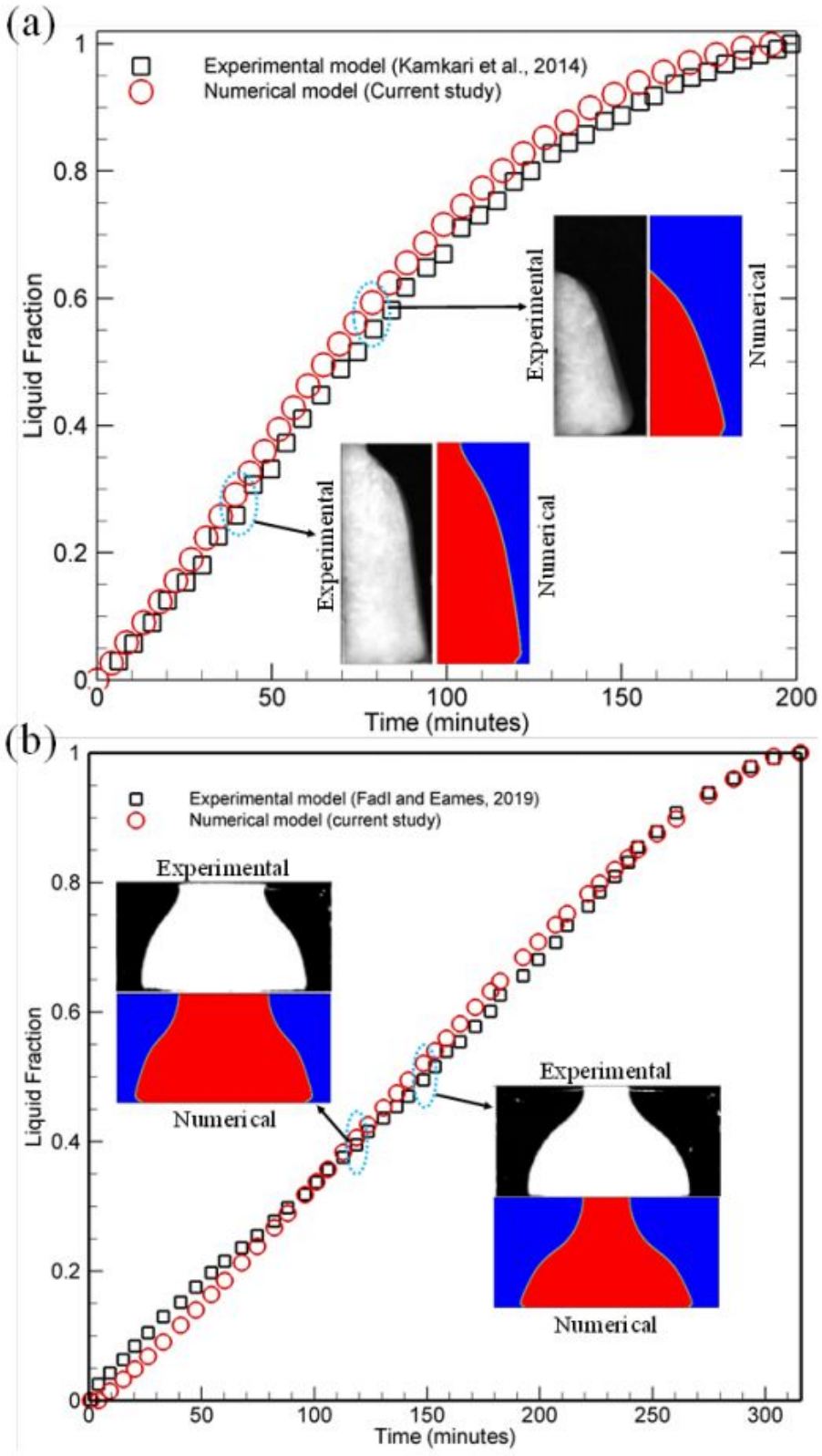

Figure 6.4: Comparison of liquid fraction – time curve between numerical and experimental model for (a) conventional mono-facial heating of PCM , and (b) bifacial heating of PCM . Solid-liquid interface patterns are given in inset for specified time.

to the development of convection current in mixed regime of melting. In quasi-steady convection mode of melting, convection current develops in the overall liquid region of the enclosure, and solid-liquid interface propagation is no longer parallel to the PV panel. The domination of convection current is more in the upper region due to significant buoyant forces than the lower region, which can be seen in solid-liquid interface contour at 60 minutes in Figure 6.5(a). The solid shrinking melting regime starts when the melting front approaches the bottom wall (at 90 minutes). In this melting regime, the strength of convection current starts to diminish in the upper region due to thermal stratification, and melting slows down. The shrinking of solid along the bottom wall is visible at 120 minutes.

Melting in BIF-PV/PCM system initiates from both sides (top and bottom wall), and the melting front is similar in conduction mode of melting. Nevertheless, convection current differs for the bottom wall heating as liquid fraction rises against the solid-liquid interface and deteriorates interface in both upper and lower region. In contrast, the interface is eroded from the upper side only for the top PV panel in mixed mode melting (at 30 minutes). The development of convection current initiates small convection current loops (Benard convection loops) due to low angle (25°) of inclination with horizontal and bottom wall heating. The structure of solid-liquid interface towards bottom PV panel in Figure 6.5(b) at 60 minutes shows the Benard convection loops while top PV panel shows similar melting as in PV/PCM system. The quasi-steady convection mode of melting ends when the melting front from both sides interacts at 55 minutes of the process and gives rise to solid-shrinking mode; however, the solid does not shrink along the bottom wall at this juncture. It can be seen at 90 minutes that most of the PCM gets melted. After complete melting of PCM, heat is stored in a sensible form, and the average temperature of PCM increases, increasing the temperature of the PV panel and degrades its performance. Hence, the thickness of the PCM enclosure is increased by 10 mm in PV/PCM system and BIF-PV/PCM system in Figures 6.5(c) and 6.5(d), respectively.

PV/PCM system in Figure 6.5(c) exhibits similar melting behavior as PV/PCM system in Figure 6.5(a), except it does not show the end of the quasi-convection melting regime during the melting process. Moreover, the melting morphology of the L_{30} BIF-PV/PCM system is similar to L_{20} BIF-PV/PCM system, but the quasi-convection regime of melting extends to 85 minutes, resulting in more latent heat storage and allowable heat storage PV panels to work at a relatively lower temperature. Figure 6.5(e) shows the melting front contours for the modified BIF-PV/PCM system (V_L/V_R = 16/14) with the same volume as the L_{30} BIF-PV/PCM system. The modified non-rectangular enclosure increases the quasi-steady convection mode of melting by adjusting more PCM in the upper part of the enclosures. Benard convection loops dominate in the bottom enclosure, but that was not the case in the top enclosure; hence, the designs of both the enclosure need not be similar. PCM is more uniformly distributed in the lower and upper half of the bottom enclosure as melting is uniform due to Benard convection loops. The top enclosure is designed to have more PCM in the upper part of the enclosure. Such designs are made to follow

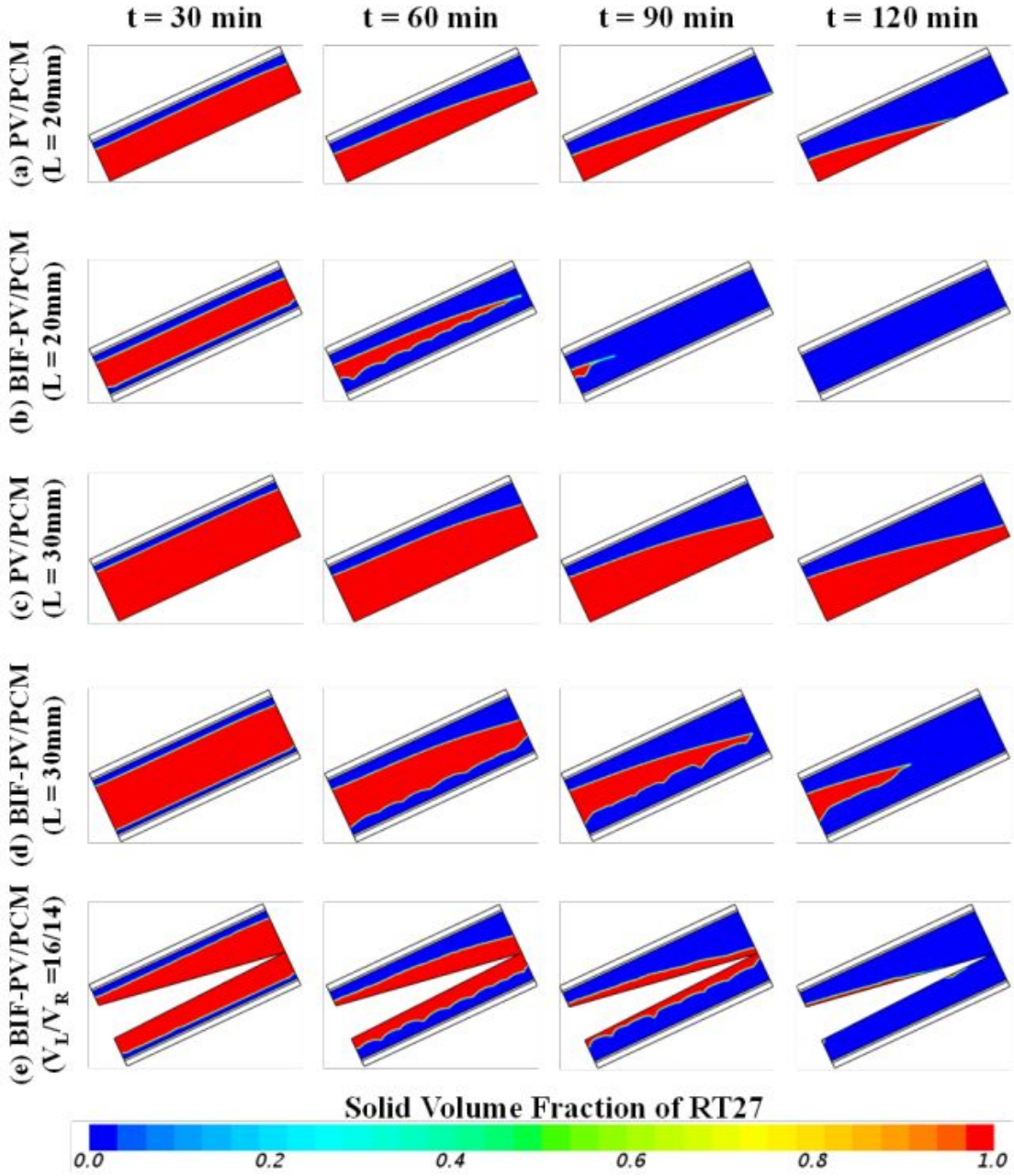

Figure 6.5: Solid-liquid interface patterns for PV/PCM systems and BIF-PV/PCM systems.

convection-dominated melting. The quasi-convection melting regime extends to 105 minutes of the process and absorbs more heat as latent heat, making both PV panels work at lower and relatively constant temperatures.

6.3.2 Temperature distributions

Figure 6.6 demonstrates the spread of sensible heat in PV/PCM systems and BIF-PV/PCM systems with the help of temperature distribution contours. Absorption of more sensible heat by

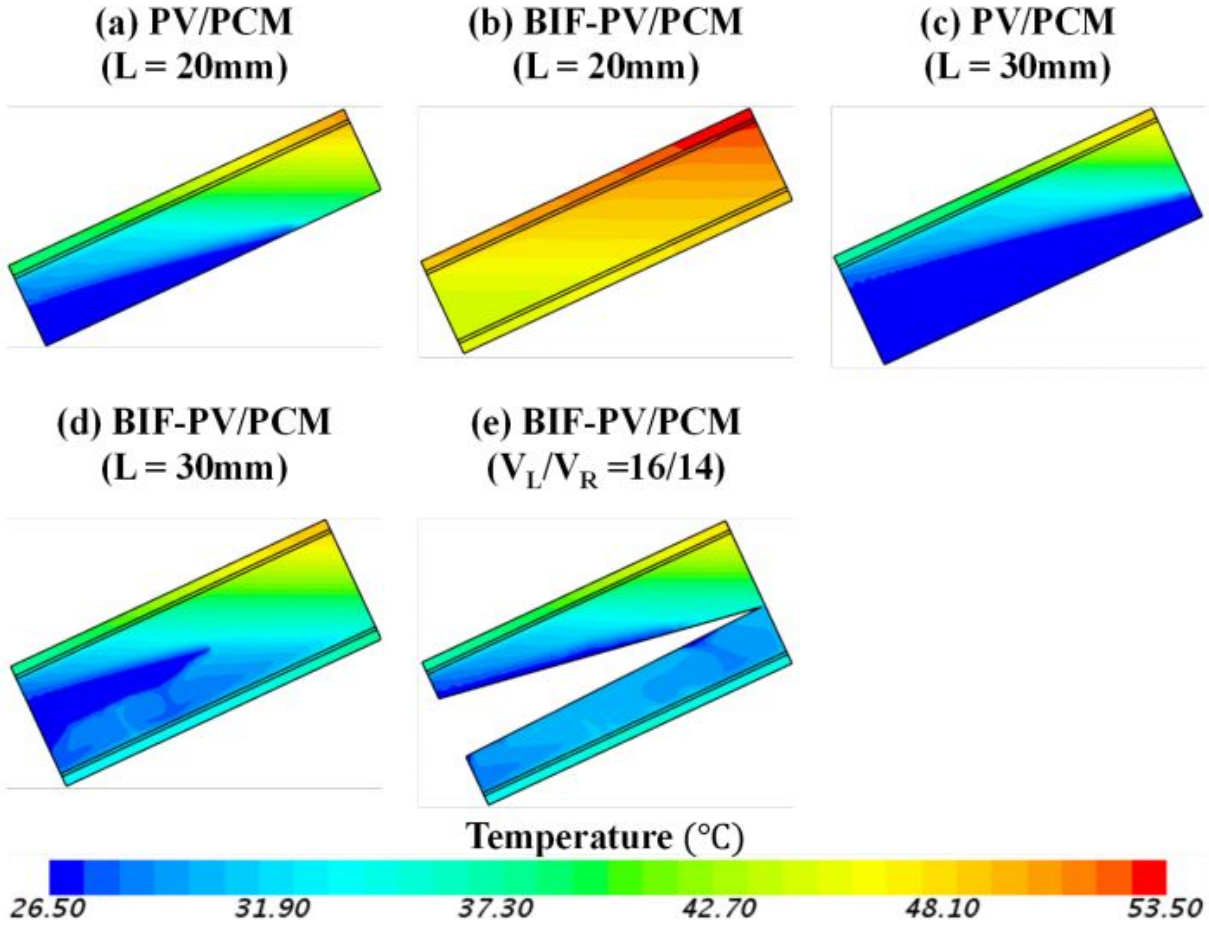

Figure 6.6: Temperature distribution at 120 minutes for PV/PCM systems and BIF-PV/PCM systems.

PCM indicates the increase of temperature of PCM, and subsequently, the temperature of the PV panel also increases. PCM absorbs sensible heat in a solid-state and liquid state while it absorbs latent heat during phase change. Hence, the melting morphology of PCM decides the temperature distribution within the cavity. The development of convection current fastens the melting in the upper part of the enclosure, and slow melting is observed in the lower part of the enclosure. Thus, liquid PCM starts absorbing heat in the sensible form in the upper part earlier than the lower part. Non-uniform melting in rectangular PCM enclosure is responsible for non-uniform temperature distribution in PCM enclosure and PV panel in PV/PCM systems and BIF-PV/PCM systems. Figure 6.6(a) demonstrates temperature distribution in L_{20}PV/PCM system. It is observed that temperature distribution is according to discussed melting morphology.

The maximum temperature in the top left corner of the PCM enclosure is 49.23°C, which causes PV temperature to rise to a maximum value of 50.53°C in the same corner. The lower region temperature is maintained to a low value due to the presence of solid PCM. The bottom PV panel and reflected radiation to the system increase the heat input, accelerating the melting pro-

cess and increasing the sensible content in the enclosure after the complete melting of PCM. The maximum temperature in the enclosure is 52.97°C, which causes the maximum temperature of the top PV panel to rise to 53.49°C and the bottom PV panel to 49.42°C in the L_{20} BIF-PV/PCM system shown in Figure 6.6(b). PV/PCM system with increased PCM thickness ($L = 30mm$) exhibits quasi-steady mode of melting till 120 minutes, and so, the maximum temperature in PCM enclosure drops to 46.74°C due to which maximum PV panel temperature reduced to 48.01°C (see Figure 6.6(c)). In theL_{30} BIF-PV/PCM system, the maximum temperature within the PCM enclosure increases to 48.11°C due to increased incident radiation that causes the maximum temperature of the top PV panel to approach 49.23°C and bottom PV panel 36.41°C, as shown in Figure 6.6(d). This improvement is due to increased latent heat storage. Figure 6.6(e) demonstrates the temperature distribution for the modified BIF-PV/PCM system ($V_L/V_R = 16/14$) with same amount of PCM as in the L_{30} BIF-PV/PCM system. The enclosure is designed according to the propagation of the melting front for higher latent heat content than the sensible part.

Consequently, the maximum temperature of the PCM enclosure drops to 46.34°C in the top-left region, which reduces the maximum temperature of the top PV panel to 47.69°C and the bottom PV panel to 32.54°C. The design modification of the PCM enclosure exhibit a significant improvement in the thermoelectric performance of the system by maintaining a more uniform temperature distribution in the enclosure and increased latent content of heat storage due to faster melting. This new design allows the modified BIF-PV/PCM system to generate additional electric power and work as an efficient latent heat storage device.

6.3.3 Heat transfer characteristics

6.3.3.1 Melting process

The melting phenomenon can be visualized by plotting liquid fraction with time, as shown in Figure 6.7(a). Melting in any enclosure consists of conduction, mixed, quasi-convection, and solid shrinking heat transfer regime. Liquid fraction varies linearly with time for the first three melting regimes except the solid shrinking regime in which melting slows down due to retardation of a convection current. Liquid fraction exhibits a curvilinear trend with time in the solid shrinking regime of melting. In L_{20} PV/PCM system, the quasi-steady convection regime ends at 90 minutes. Hence, the liquid fraction loses its linearity trend after this mode as the solid shrinking regime continues subsequently. Therefore, PV/PCM system exhibits that only 73.07% of PCM gets melted during 120 minutes (duration of incident radiation). Another PV panel is added to the bottom side of the enclosure, and nearby radiation reflected by mirrors is incident on it. Hence, this BIF-PV/PCM system has increased heat input for the PCM enclosure that fastens the melting procedure and quasi-convection mode ends (interaction of top and bottom melting front) at just 55 minutes, with complete melting happens at 92 minutes of the process.

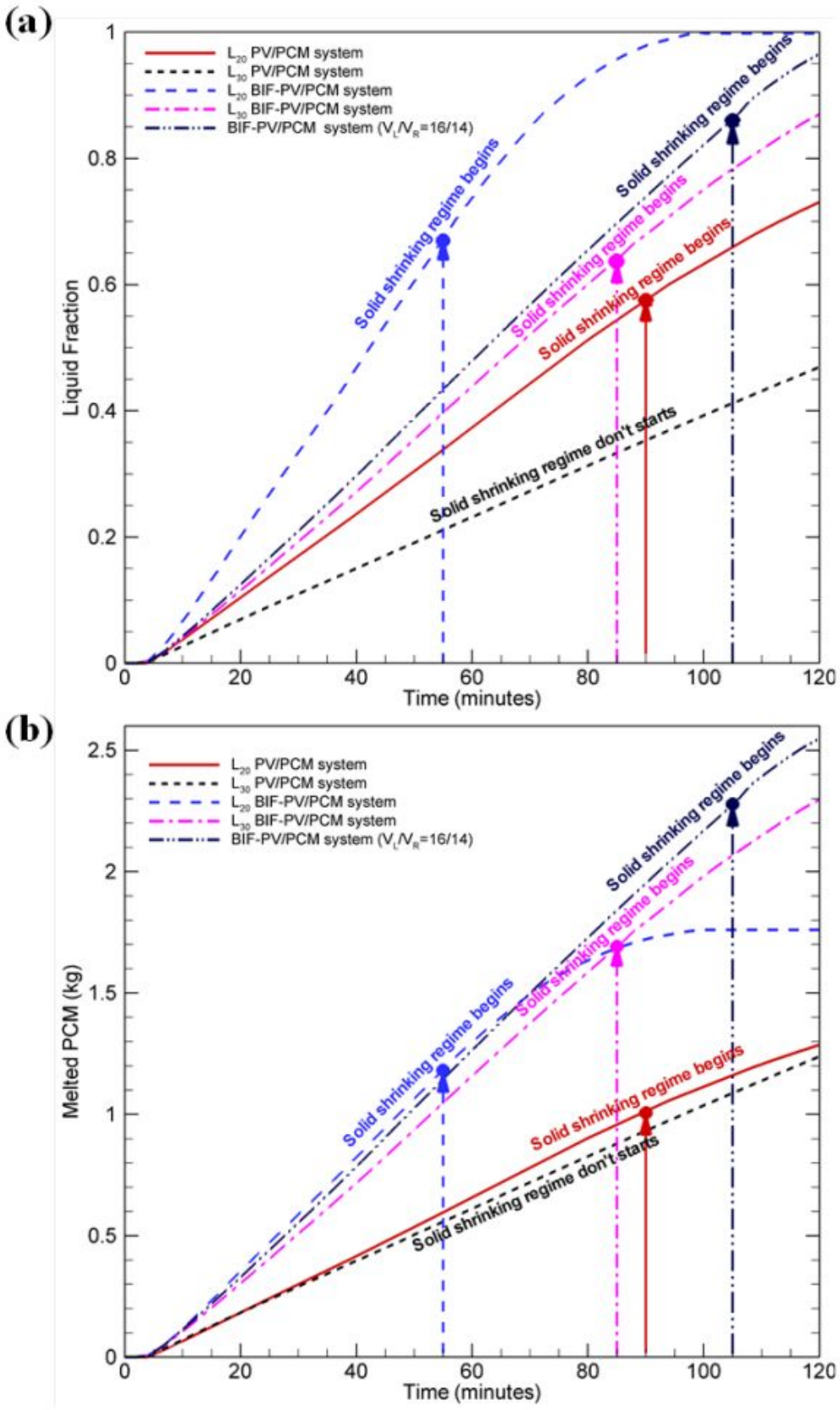

Figure 6.7: Variation of (a) liquid fraction with time, and (b) absolute amount of melted PCM with time.

After complete melting, liquid PCM starts absorbing sensible heat. Therefore, the thickness of the PCM enclosure is increased to 30 mm in BIF-PV/PCM and PV/PCM systems to ensure the storage of this extra heat input. In PV/PCM system, the trend of transient variation of liquid fraction is linear as the quasi-convection mode of melting never ends during 120 minutes, and 46.91% melting is observed. In L_{30} BIF-PV/PCM system, the span of the quasi-convection mode of melting extends to 85 minutes. Hence linearity trend of liquid fraction is enhanced for a longer time, and more latent heat content is absorbed with an enhanced melting rate. 86.98% melting is observed. In a modified BIF-PV/PCM system (V_L/V_R = 16/14), the enclosure is designed to make most of the PCM available for quasi-steady convection mode of melting. Hence, the duration of linear variation of liquid fraction with time increases to 105 minutes of the process. With the increase in period of the quasi-convection regime, the melting fraction of PCM enhanced to 96.53%, which is 10.98% higher than simple L_{30} BIF-PV/PCM system with the same volume of PCM.

The transient variation of absolute melted PCM per unit enclosure depth is plotted in Figure 6.7(b) to better understand the melting process. Different amounts of PCM are stored in the enclosure, i.e., 1.76 Kg per unit depth in the L_{20} systems and 2.64 Kg per unit depth in the L_{30} systems. The trends of transient variation of absolute melted PCM are similar to the liquid fraction. In L_{20} PV/PCM system, 1.286 kg of PCM entirely melted during 120 minutes of the process, which decreases by 3.69% in the L_{30} PV/PCM system (1.238 kg) due increase in sensible heat storage. In L_{20} BIF-PV/PCM system, all of the PCM (1.76 Kg) melted in just 92 minutes out of 120 minutes, and most of the heat is stored as sensible heat, which increases the temperature of both the PV panel. The addition of the bottom PV panel and reflected radiation accelerates the melting process, but the 20 mm enclosure does not have sufficient PCM to store this increased heat content in latent form. The L_{30} BIF-PV/PCM system is used to drop down the sensible heat content of the PCM enclosure, and it is observed that 2.296 Kg of PCM melted during 120 minutes of the radiation activity. For further performance enhancement, the rectangular enclosure is replaced by a modified non-rectangular cavity designed according to melting morphology. Hence, melting is further enhanced by 10.98% and 2.549 Kg of PCM melted during the process of 120 minutes. The melted PCM in modified BIF-PV/PCM system (V_L/V_R = 16/14) is 1.98 times the melted PCM in the L_{20} PV/PCM system and 2.05 times of melted PCM in the L_{30} PV/PCM system. In addition to increased latent heat content, the modified system also ensures the enhanced electric performance of the PV panel by reducing PV panel temperature and letting the panel work close to reference conditions. Hence modified BIF-PV/PCM system (V_L/V_R = 16/14) is more efficient design for better thermo-electric performance.

6.3.3.2 Nusselt number

Nusselt number indicates the strength of heat transfer to the fluid from any surface or boundary. Figure 6.8 represents the transient variation of the Nusselt number at the top PV-PCM interface for PV/PCM and BIF-PV/PCM systems. At any instant of time, Nusselt number (Nu) along the top PV-PCM interface can be given by Eq. 2.15.

In the conduction regime of melting, the value of the Nusselt number is very high. Nusselt number starts to decrease with an increase in thickness of liquid PCM in conduction mode of melting. Soon, buoyant forces start to develop, giving rise to a mixed melting regime, and the Nusselt number still decreases until buoyant forces overcome the viscous forces. After this, the Nusselt number begins to rise to the development of convection current in the entire liquid region, giving rise to the quasi-steady convection regime of melting. Nusselt number is approximately constant in this regime. In the solid-shrinking melting regime, the Nusselt number decreases linearly due to the retardation of convection current.

The L_{20} PV/PCM system and L_{30} PV/PCM system shows the above-discussed trend for Nusselt number (see Figure 6.8). However, the L_{30} PV/PCM system exhibit an improvement of 33.92% compared to the L_{20} PV/PCM system at the end of 120 minutes as the quasi-convection regime of melting never ends for this configuration. In BIF-PV/PCM system, the trend of transient variation of Nusselt number is similar to PV/PCM system except for that quasi-convection regime of melting ends here with the interaction of both the melting fronts. Nusselt number curve exhibit a spike for the top PV/PCM interface. This spike arises due to different heat contents of the upper and lower melting front, causing the difference in the average temperature of liquid PCM in the upper and lower melting front. For L_{20} BIF-PV/PCM system, the quasi-convection mode of melting ends very soon (55 minutes), and therefore, a spike is visible in the Nu-time curve at 55 minutes, and the Nusselt number starts to decrease in solid-shrinking mode till 92 minutes where complete melting of PCM takes place. Nusselt number decreases rapidly after total melting due to thermal stratification caused by sensible heating of liquid PCM and reaches a low value at 120 minutes. Increasing PCM thickness to 30 mm delays the interaction time of both melting fronts to 85 minutes, and the Nusselt number depicts the similar trend of Nusselt number as in L_{20} BIF-PV/PCM system. However, complete melting of PCM does not occur here due to the increase in PCM amount. In L_{30} BIF-PV/PCM system, the Nusselt number exhibits an improvement of 533.86% (at 120 minutes) compared to L_{20} BIF-PV/PCM system as the duration of the quasi-steady regime of melting increases by 54.54%, and less thermal stratification is observed due to increased amount of PCM. By modifying the design of PCM enclosure according to the propagation of melting front in modified (V_L/V_R = 16/14), the duration of quasi-convection mode is further increased to 105 minutes which is an enhancement of 23.53% compared to the L_{30} BIF-PV/PCM system and 90.91% compared to L_{20} BIF-PV/PCM system. The Nusselt number (at 120 minutes) is enhanced by 23.67 % compared to theL_{30} BIF-PV/PCM

system and 683.95% compared to the L_{20} BIF-PV/PCM system, a significant improvement.

In addition to the top PV panel, reflected radiation is also incident on the bottom PV panel of the BIF-PV/PCM system. Therefore, the bottom PV-PCM interface is also a heat absorption wall for PCM enclosure, and Nusselt number variations must be understood on this wall. Figure 6.8(b) exhibits the transient variation of the Nusselt number on the bottom PV-PCM interface for all discussed BIF-PV/PCM systems. The Nu-time curve exhibits a similar trend for the bottom PV-PCM interface as shown for the top PV-PCM interface in the conduction melting regime. With the start of convection current from the bottom interface, small Benard convection loops form that accelerate the heat transfer in the mixed melting regime. Nusselt number approaches a local minimum value as conductive heat transfer ends, and convective heat transfer dominates the entire liquid region, leading to the quasi-convective melting regime. Small Benard loops merge to form larger loops with the development of convective melting. In this mode, the Nusselt number is nearly invariable with time, and this mode ends with the interaction of both melting fronts where the Nu-time curve exhibit a sudden kink or reduction, and then the Nusselt number starts to decrease in solid-shrinking mode. This sudden kink in the $Nu-time$ curve for the bottom wall is concurrent with the sudden spike for the top wall. These sudden peaks and kinks in the $Nu-time$ curve for top and bottom walls arise due to the interaction of top and bottom melting fronts with different input heat fluxes for top and bottom PV panels. In L_{20} BIF-PV/PCM system, the $Nu-time$ curve follows the same trend where complete melting of PCM takes place at 92 minutes, after which the Nusselt number decreases drastically due to thermal stratification. In the L_{30} BIF-PV/PCM system, the quasi-convection regime of melting delays up to 85 minutes, making the Nusselt number rise many times of the previous system. In modified BIF-PV/PCM system ($V_L/V_R = 16/14$), the design of the enclosure is to promote convective melting, and hence, the average Nusselt number increases by 8.99% compared to L30 BIF-PV/PCM system except for the fact that Nusselt number drops a little for modified design in last few minutes due to thermal stratification of liquid PCM.

The enhancement of the Nusselt number indicates dominance in convective heat transfer mode in the enclosure. Hence, it is established that modified BIF-PV/PCM system absorbs more latent heat content as PCM is distributed according to convection current and thus, providing uniform temperature distributions and better thermo-electric performance.

6.3.4 Performance characteristics

6.3.4.1 Effect of PV cell temperature on power conversion efficiency

The temperature of the PV panel affects the power or electrical conversion efficiency of the PV panel, according to Eq. 2.14. The elevated temperatures ensure the working of the PV panel far away from the reference working conditions. The electrical performance of the PV panel degrades as its operating temperature deviates from the reference temperature. PV panel (c-Si)

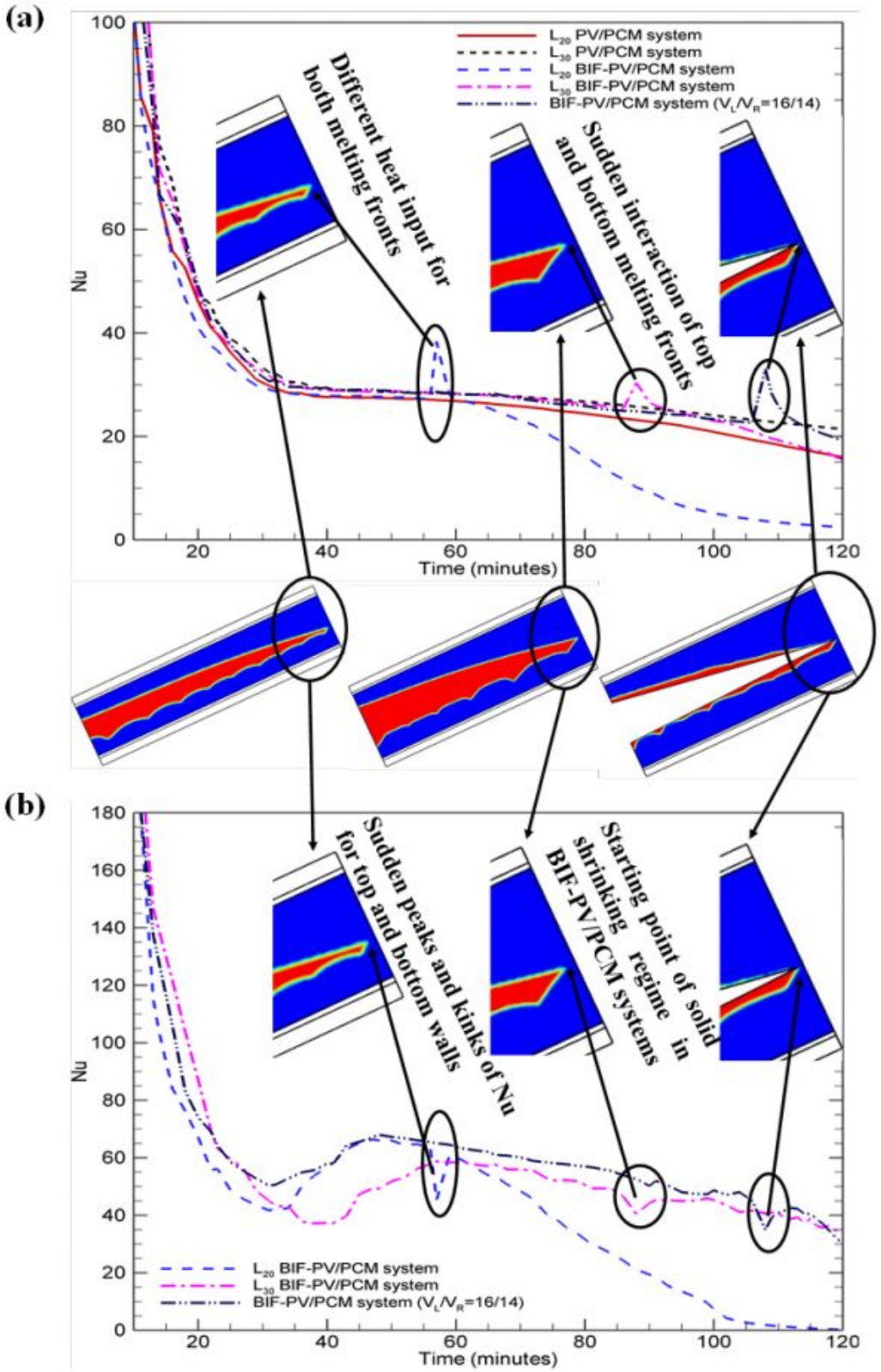

Figure 6.8: Variation of (a) Nusselt number for top PV-PCM interface with time for PV/PCM systems and BIF-PV/PCM systems (b) Nusselt number for bottom PV-PCM interface with time for BIF-PV/PCM systems. Solid-liquid interface patterns at peaks and kinks are shown in inset.

considered for this case has a reference temperature of 25°C and 12.4% as reference electrical conversion efficiency. PCM enclosure is attached to cool down the PV panels by absorbing heat and make them work near reference temperature. The temperature of the PV panel rises to 56.78°C in the PV system and BIF PV system, respectively, which causes electric conversion efficiency to fall to 10.84% and 10.69% for the respective system. In L_{20} PV/PCM system, the temperature of the PV panel is elevated to 41.63°C, which causes electrical conversion efficiency to fall to 11.58%. Using a rectangular PCM enclosure of thickness 30 mm, PV panel temperature reduces slightly to 39.33°C, and electrical efficiency improves marginally to 11.69%. The reflected radiation increases the heat input in the case of bifacial PV systems that fastens the melting process while the heat-absorbing capacity of PCM remains the same. Hence, the elevation of PV panel temperature is quite certain; however, it has been demonstrated in this paper that suitable design changes can decrease the PV panel temperature significantly. The transient variation of PV panel electrical conversion efficiency for top and bottom PV panels is shown in Figure 6.9. In L_{20} BIF-PV/PCM system, the temperature of the top and bottom PV panel rises to 50.64°C and 46.82°C, respectively. This significant deviation from reference temperature is due to sensible heat gain by PCM after complete melting. Therefore, the electrical conversion efficiency of top and bottom PV panels reduces to 11.14% and 11.33%, respectively.

In theL_{30} BIF-PV/PCM system, additional PCM absorbs heat in latent form and reduces the PV panel temperature to 41.25°C for the top PV panel and 33.08°C for the bottom PV panel. This reduction in temperature improves the electrical efficiency to 11.60% and 12% for top and bottom PV panels, respectively. Further, the enclosure design is improved to a non-rectangular shape (BIF-PV/PCM system (V_L/V_R = 16/14)), allowing more PCM in the convection-dominated region that reduces the temperature of the top PV panel to 39.77°C and 32.92°C for the bottom PV panel, respectively. The electrical conversion efficiency was enhanced to 11.68% for the top PV panel and 12.01% for the bottom. By modifying the enclosure's design, the electrical performance of the top PV panel in the BIF-PV/PCM system (V_L/V_R = 16/14) is matched with the L_{30} PV/PCM system even in the presence of increased heat input for the PCM cavity. Moreover, the power output from the bottom PV panel is an added advantage to the system. The sudden peaks and kinks are seen in the electric conversion efficiency of top, and bottom PV panels, respectively, at the end of the respective quasi-convection regime in all BIF-PV/PCM systems. These peaks and kinks are due to the interaction of melting fronts of different energy contents, and their effect on the performance of the PV panel is significant but for a concise duration. It is evident that bifacial systems are more efficient than simple PV/PCM systems except for the L_{20} BIF-PV/PCM system, which shows deterioration in efficiency after the end of quasi-convection mode and after complete melting.

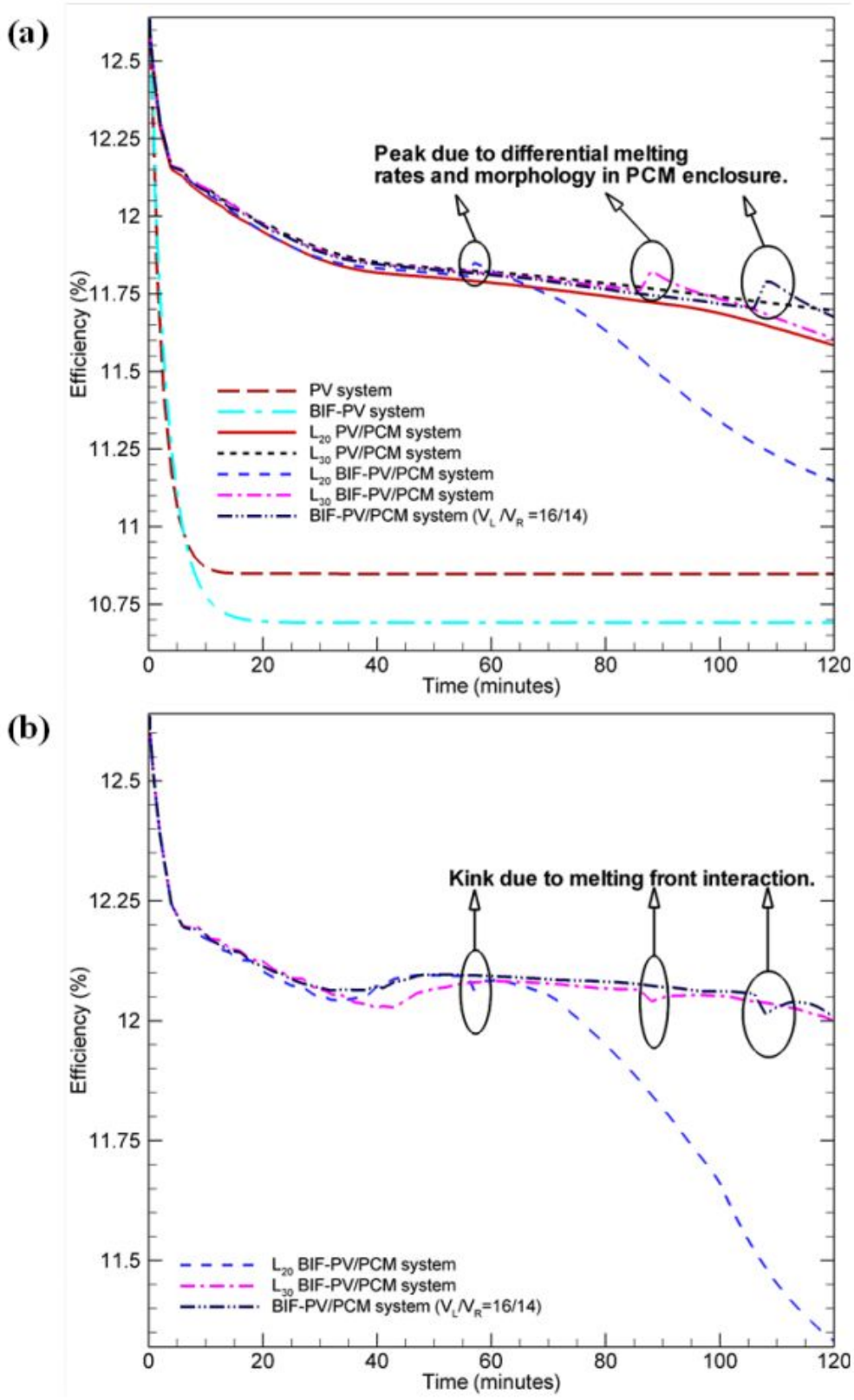

Figure 6.9: Transient variation of PV cell electric conversion efficiency of (a) top PV panel, and (b) bottom PV panel for all configurations of PV and PV/PCM systems.

6.3.4.2 Total electric power output

Figure 6.10 demonstrate the variation of power output per unit area of PV panel with time for all configurations of PV//PCM systems and BIF-PV/PCM systems. Electric power output per unit area at any instant of time can be defined as the sum of electric power output of top and bottom PV panels:

$$P_{out} = P_{out,top} + P_{out,bottom} \tag{6.6}$$

where the power output of the top PV panel for both types of configurations (PV//PCM systems and BIF-PV/PCM systems) is defined as:

$$P_{out,top} = \eta_{pv,top}\alpha_{pv}\tau_g I_{solar} \tag{6.7}$$

For PV/PCM systems, there is no bottom PV panel; hence electric power output for bottom PV panel ($P_{el,bottom}$)is zero, while for BIF-PV/PCM systems, the electric power output of the bottom PV panel is defined as:

$$P_{out,bottom} = \eta_{pv,bottom}\alpha_{pv}\tau_g I_{solar}^{reflected} \tag{6.8}$$

Power output exhibits similar variation with time as that of electrical conversion efficiency. Initially, the electric power output is maximum and equal to reference power output, and it decreases with an increase in the temperature of the PV panel. The electric power output drops to 74.02 W/m^2 (at 120 minutes) from 86.43 W/m^2 (at the beginning) as the temperature of the PV panel rises to 56.78°C in the conventional PV system. In PV/PCM systems, the temperature of the PV panel is controlled by the melting morphology of PCM. Therefore, power output is also regulated by the melting behavior of PCM. Both L_{20} PV/PCM system and L_{30} PV/PCM system exhibit the same power output till the end of quasi-regime in the L_{20} PV/PCM system. After that, It shows a continuous reduction in electric power with time. L_{20} PV/PCM system exhibits a power production rate of 79.23 W/m^2 at the end of 120 minutes. The L_{30} PV/PCM system possesses 80.01 W/m^2 as quasi-regime never ends for 30 mm enclosure during the radiation activity. The bottom PV panel and reflected radiation significantly boost power output in all BIF-PV and BIF-PV/PCM systems.

Initially, the BIF-PV system exhibited a power output of 151.25 W/m^2, which decreased to 127.98 W/m^2 by 120 minutes due to a rise in PV panel temperature (60.01°C). In BIF-PV/PCM systems, characterization of melting controls the electric performance of PV panels by stabilizing their operating temperature. In the L_{20} BIF-PV/PCM system, the power output was maintained at 142.85 W/m^2 until the end of the quasi-convection regime of melting (55 minutes). After that, it decreases in the solid-shrinking regime and further decreases to 134.37 W/m^2 by the end of 120 minutes as sensible heat gain after complete melting increases the temperature

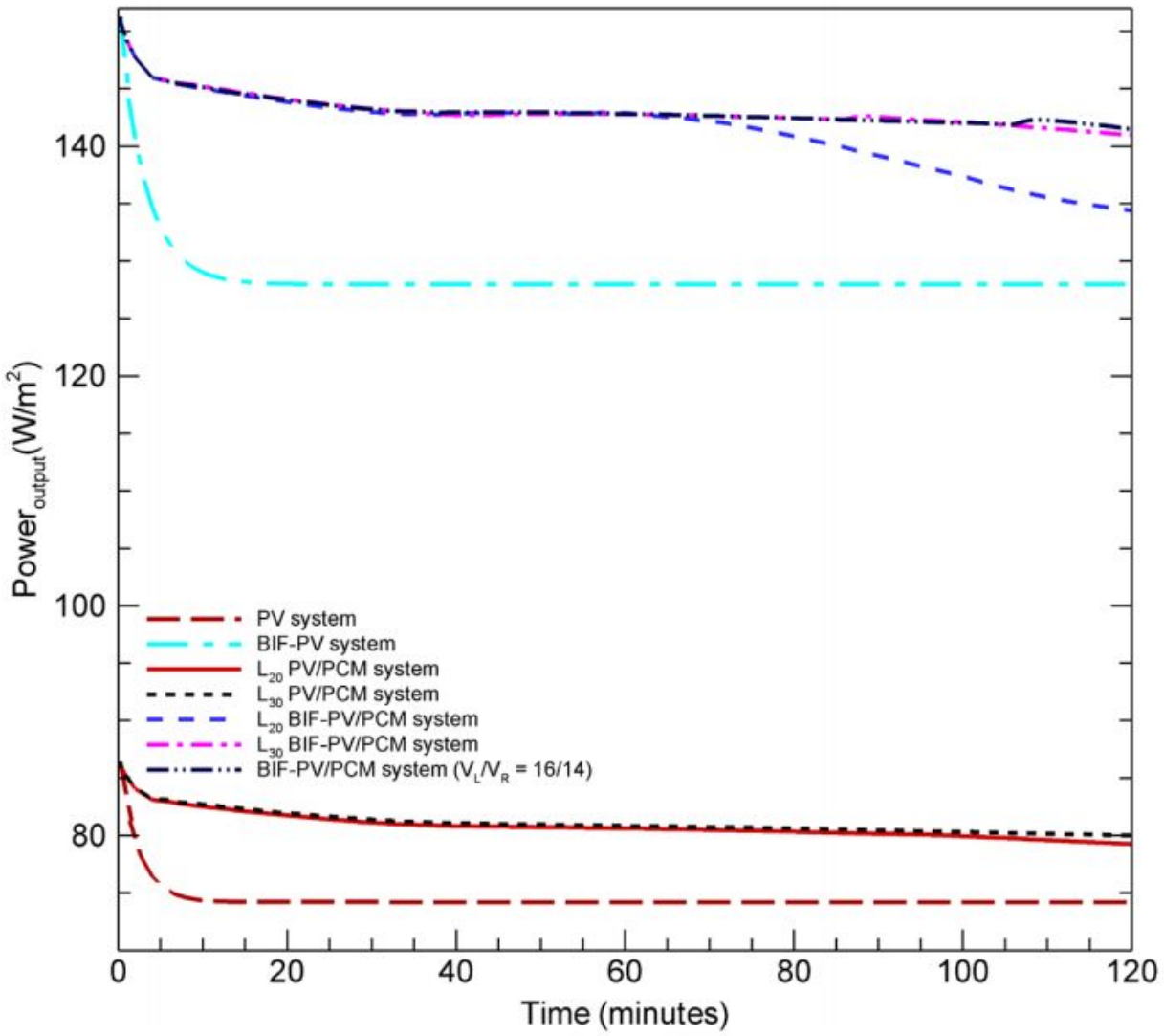

Figure 6.10: Variation of overall electric power output with time for different configurations of PV and PV/PCM systems.

of both the PV panels. Additional PCM in the L_{30} BIF-PV/PCM system enhances the duration of the quasi-convection regime of melting and thus, increases the power output to 140.02 W/m^2 by decreasing the PV panel temperature for the top-bottom PV panel.

Further modification of enclosure in BIF-PV/PCM system (V_L/V_R = 16/14) enhances the quasi-convection mode of melting for a longer duration, and hence, electric power output is enhanced to 141.45 W/m^2 by 120 minutes. Moreover, BIF-PV/PCM system (V_L/V_R = 16/14) produces 78.53% more electric output than the simple L_{20} PV/PCM system, 76.79 % more than L_{30} PV/PCM system, and 5.27 % more than L_{20} BIF-PV/PCM system. The electric power output is marginally enhanced in the modified BIF-PV/PCM system, but at the same time, it absorbs more heat compared to the simple BIF-PV/PCM system of the PCM enclosure of the same volume.

Table 6.1: Equations for energy efficiency and exergy efficiency analysis .

Energy efficiency analysis

Total solar energy input (E_{total}):

$$E_{total} = \int_{t_1}^{t_2} \alpha_{pv}\tau_g G A_{pv} dt \tag{6.9}$$

where A_{pv}: Area of PV panel, $G = I_{solar}$ for mono-facial systems, $G = I_{solar} + I_{solar}^{reflected}$ for bifacial systems,

Utilized electrical energy (E_{el}):

$$E_{el} = \int_{t_1}^{t_2} P_{out} * A_{pv} dt \tag{6.10}$$

Utilized thermal energy (E_{th}):

$$E_{th} = m_p(C_p\Delta T + f_l L_{sf}) \tag{6.11}$$

Overall utilization energy ($E_{overall}$):

$$E_{overall} = E_{el} + E_{th} \tag{6.12}$$

Overall energy efficiency ($\eta_{overall}$):

$$\eta_{overall} = E_{overall}/E_{total} \tag{6.13}$$

6.3.4.3 Overall system performance

The overall performance of the system can be estimated by its potential to utilize input energy. Energy and exergy efficiency analysis can be the relevant tools to analyze the overall performance of the system. The equation required to calculate energy efficiency and exergy efficiency is given in Tables 6.1 and 6.2[70].

Energy efficiency analysis:

Initially, overall system efficiency equals electric conversion efficiency and increases as the melting process progresses and reaches a maximum value in the quasi-convection melting regime and then decreases in solid-shrinking mode. Further, decrement after complete melting was observed. Figure 6.11 represents the variation of overall system efficiency for different PV and PV/PCM systems configurations. PV and BIF-PV systems only produce electric energy; hence, overall system efficiency is 10.84% and 10.69% (at 120 minutes of the process) for PV and BIF-PV systems, respectively. Overall system efficiency in the L_{20} PV/PCM system is observed at 69.91% at the end of 120 minutes, decreasing to 68.74% due to increased sensible gains in PCM for the

Table 6.2: Equations for energy efficiency and exergy efficiency analysis.

Exergy efficiency analysis

Exergy balance:

$$\sum Ex_{in} - \sum Ex_{out} = \sum Ex_{loss} \tag{6.14}$$

where Ex_{in}, Ex_{out}, and Ex_{loss} are input, output, and loss of exergy in the system.

Input exergy (Ex_{in}):

$$Ex_{in} = A_{pv}\alpha_{pv}\tau_g G[1-4/3(T_a/T_{sun})+1/3(T_a/T_{sun})^4] \tag{6.15}$$

where T_{sun} is temperature of sun (black body).

Thermal exergy (Ex_{th}):

$$Ex_{th} = m_p[C_p(T_f - T_i - T_a ln(T_f/T_i)) + L_{sf}(1-T_a/T_m)] \tag{6.16}$$

Output exergy: (Ex_{out})

$$Ex_{out} = Ex_{el} + Ex_{th} \tag{6.17}$$

Electrical exergy (Ex_{el}) is 100%.

Total exergy efficiency (η_{ex}):

$$\eta_{ex} = Ex_{out}/Ex_{in} \tag{6.18}$$

L_{30} PV/PCM system. There is no reflected radiation for PV/PCM systems, but for BIF-PV/PCM systems, reflected radiation enhances the heat input to the enclosure. In L_{20} BIF-PV/PCM system, increased heat input enhances the melting rate and quasi-convection mode of melting ends soon that causes the latent heat-absorbing capacity of the system to decay and then diminish after complete melting. Hence, overall stage efficiency after significant losses degraded to 60.23% by 120 minutes.

Further enlarging the thickness of the PCM enclosure to 30 mm, removes the limitations of the L_{20} BIF-PV/PCM system, and overall stage efficiency improves to 68.75% in L_{30} BIF-PV/PCM system. The improvement in the design of the PCM enclosure (by making it non-rectangular) enhances the melting rates by availing more PCM for the convection-dominated region in BIF-PV/PCM system (V_L/V_R = 16/14). Therefore, overall system efficiency increases and approaches 73.71%, which is quite significant and allows the modified BIF-PV/PCM system to utilize 87.65% more incoming radiation than conventional PV/PCM system. The improvement in overall system efficiency in the modified BIF-PV/PCM system is 5.43% more than L_{20} PV/PCM system, 7.23% more than L_{30} PV/PCM system, 22.38% more than L_{20} BIF-PV/PCM system, and 7.21% more thanL_{30} BIF-PV/PCM system, respectively. Hence, the modified BIF-PV/PCM system exhibits a significant enhancement in overall performance.

Exergy efficiency analysis:

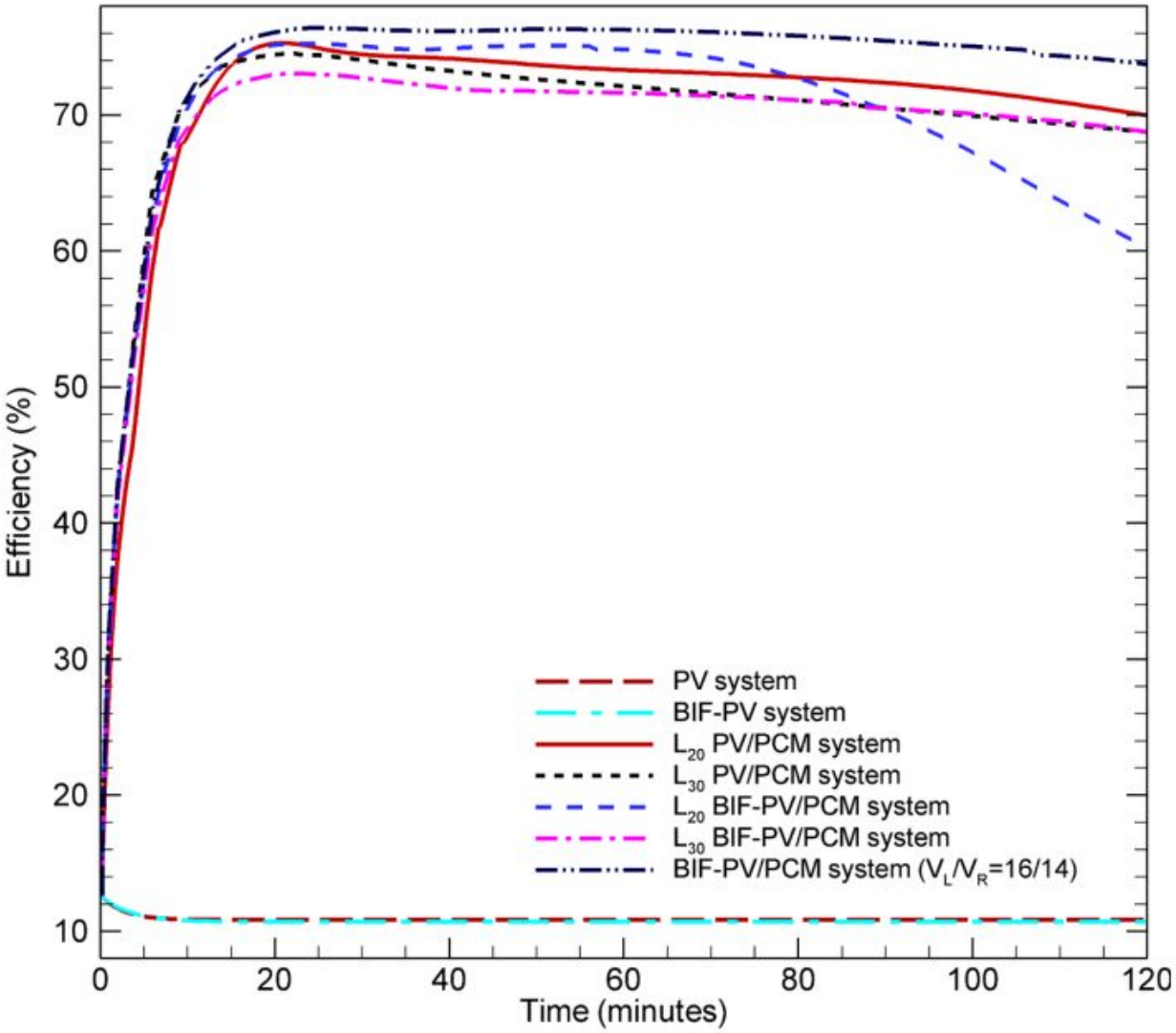

Figure 6.11: Variation of overall system efficiency with time for different configuration of PV and PV/PCM systems.

Exergy is the valuable part of the total utilized energy of a system. Exergy is an indication of the quality of energy.

Figure 6.12 shows the exergy efficiencies for different configurations of PV and PV/PCM systems. In contrast to thermal energy, the exergy efficiency of thermal energy is much smaller than the exergy of electrical energy for PV/PCM systems and BIF-PV/PCM systems. The exergy efficiency of thermal energy is zero for PV and BIF-PV systems, whereas it varies slightly in a small range of 1.35-1.53 for PV/PCM and BIF-PV/PCM systems. The results indicate that thermal management and insolation management strategies affect the exergy of electricity significantly. The total exergy efficiencies are 11.64%, 11.47%, 13.88%,13.90%, 13.53%,14.04% and 14.21% for PV system, BIF-PV system, L_{20} PV/PCM system, L_{30} PV/PCM system, L_{20} BIF-PV/PCM system, L_{30} BIF-PV/PCM system, and modified BIF-PV/PCM system ($V_L/V_R = 16/14$), respectively. The

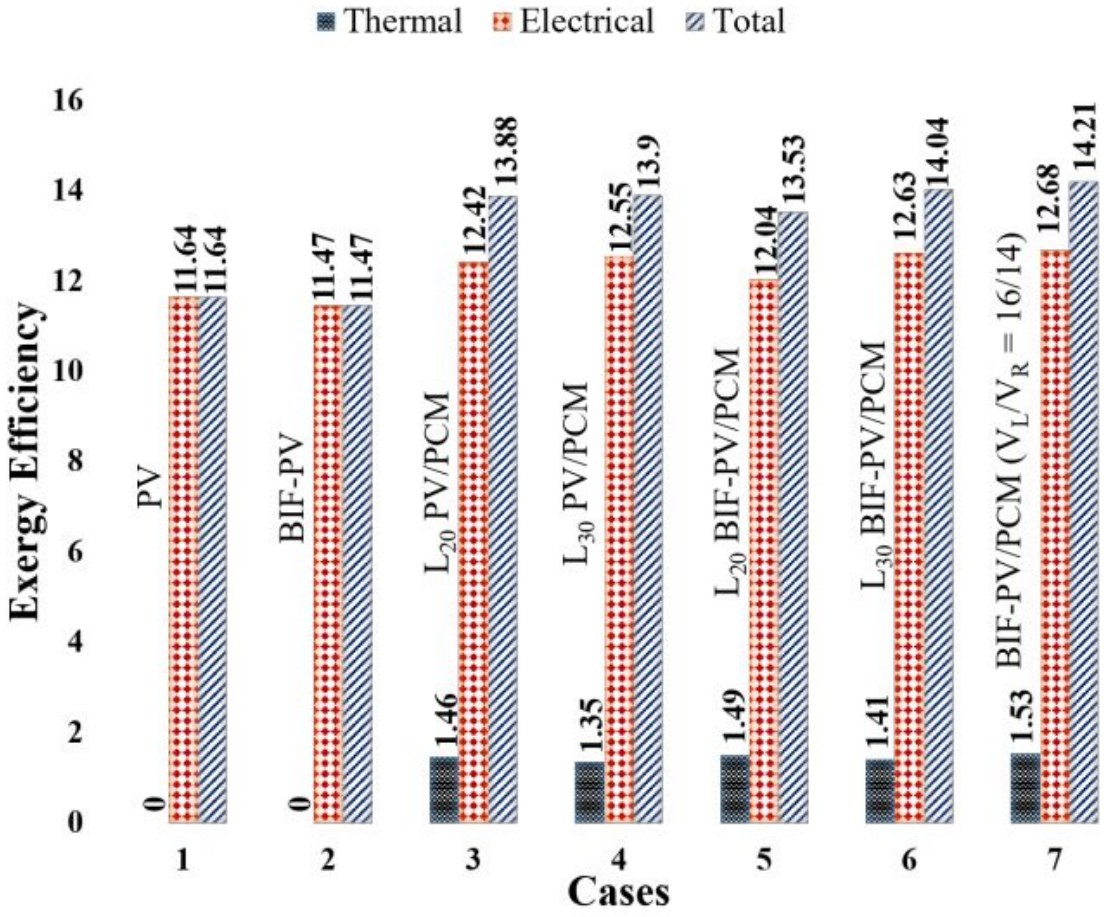

Figure 6.12: Comparison of exergy efficiency for different configurations of PV and PV/PCM systems.

exergy efficiency decreases for the BIF-PV system and L_{20} BIF-PV/PCM system compared to the PV system and the L_{20} PV/PCM system. However, a significant improvement is observed in the modified BIF-PV/PCM system ($V_L/V_R = 16/14$) by adopting better thermal management strategies (by changing the PCM enclosure design). Modified BIF-PV/PCM system ($V_L/V_R = 16/14$) exhibits 2.57% and 2.74% more exergy efficiency than conventional PV and BIF-PV systems. Therefore, it can be concluded that the performance of PV systems can be improved significantly by using intermittent isolation management and thermal management strategies.

6.3.4.4 Feasibility of the system

The idea of bifacial PV/PCM systems has certain constraints, such as land and capital requirements. Therefore, the system's feasibility can be analyzed based on economic analysis, exergoeconomic analysis, enviroeconomic analysis, power output density (power output per unit land area), and energy output density (energy output per unit land area). The feasibility study of any system predicts the viability of the system.

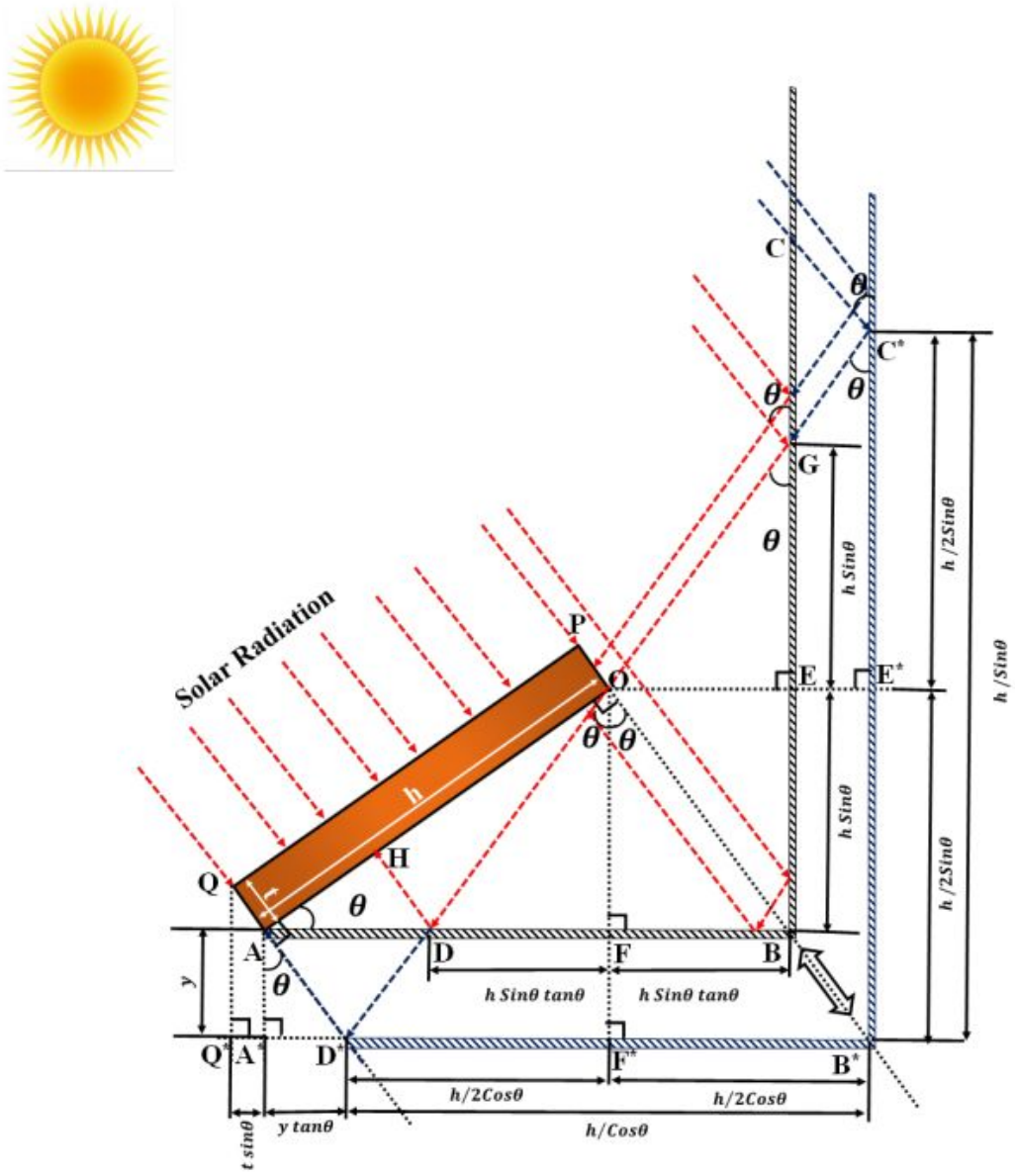

Figure 6.13: Schematic of calculation of land area requirement of integration of a single bifacial PV/PCM unit.

Power output density and energy output density:

In order to determine energy output density, the land/floor/roof area is calculated for simple PV/PCM systems and BIF-PV/PCM systems. The detailed calculation and observations for a single unit of PV/PCM system and BIF-PV/PCM system are described in Figure 6.13.

A bifacial PV/PCM unit of length h, thickness t, and unit dimension in the z-direction is inclined to an angle of θ to the horizontal, and an L shape mirror system is considered. Since the study is performed for peak radiation hours, normal radiation is assumed to fall on the PV panel. If L shape mirror system is integrated to the bottom of the PV panel, then the reflected radiation does not cover the entire face of the bottom PV panel, and length AH remains unexposed to

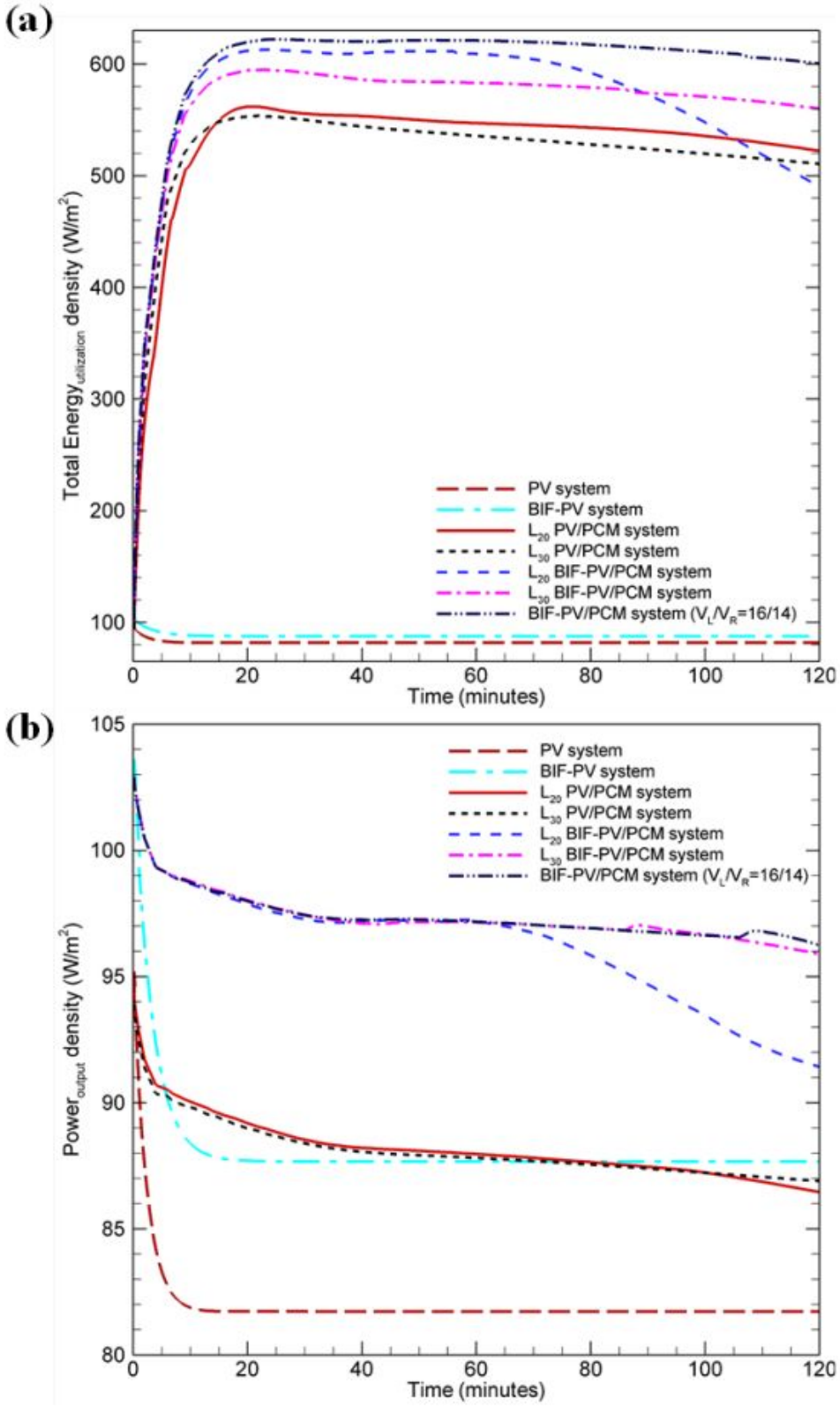

Figure 6.14: Comparison of (a) total energy utilization density, (b) power output density among bifacial PV/PCM unit, simple PV/PCM unit and conventional PV system unit.

Table 6.3: Equations for economic, exergoeconomic and enviroeconomic analysis .

Economic, Exergoeconomic, and Enviroeconomic analysis:

First annual cost (FAC):

$$FAC = CRF * C_{total} \tag{6.19}$$

where C_{total} is capital investment, and CRF is capital recovery factor.

$$CRF = \frac{i(1+i)^n}{(1+i)^n - 1} \tag{6.20}$$

where i represents interest rate, n is life span of system.

Annual salvage value (ASV):

$$ASV = SSF * S \tag{6.21}$$

where SSF indicates sinking fund factor and S is salvage value.

$$SSF = i/(1+i)^n - 1 \tag{6.22}$$

$$S = C_{total}(1 - i_d)^n \tag{6.23}$$

i_d : Depreciation rate.

Annual maintenance cost (AMC):

$$AMC = 0.15 * FAC \tag{6.24}$$

Total annual cost (TAC):

$$(TAC) = FAC + AMC - ASV \tag{6.25}$$

Annual electricity procurement cost ($AECP$): For electricity:

$$AECP_{el} = E_n * C_t \tag{6.26}$$

For exergy:

$$AECP_{ex} = Ex_n * C_t \tag{6.27}$$

where E_n and Ex_n are annual production of electricity and exergy in kWh. The average tariff of electricity (C_t) in India for domestic use is 0.06$.

Annual saving (AS) from a unit: • For electricity:

$$AS_{el} = AECP_{el} - TAC \tag{6.28}$$

For electricity:

$$AS_{ex} = AECP_{ex} - TAC \tag{6.29}$$

Annual CO_2 emission saving φ_{CO_2}:

$$\varphi_{CO_2} = \frac{(Ex_n * 2)}{1000} \tag{6.30}$$

Earned carbon credit (Z_{CO_2}):

$$Z_{CO_2} = z_{CO_2} * \varphi_{CO_2} \tag{6.31}$$

where z_{CO_2} is global carbon value which is taken as 14.5$ per ton of CO_2.

Total annual saving (TAS) from a unit:

$$TAS = Z_{CO_2} + AS_{ex} \tag{6.32}$$

Table 6.4: Economic, exergoeconomic, and enviroeconomic analysis for studied configuration of PV and PV/PCM systems.

Item	**PV**	L_{30}**PV/PCM**	L_{30}**BIF-PV/PCM**	**BIF-PV/PCM** ($V_L/V_R = 16/14$)
C_{total}(\$)	185	200	390	390
FAC(\$)	13.61	14.72	28.70	28.70
ASV(\$)	0.46	0.50	0.98	0.98
AMC(\$)	2.04	2.21	4.30	4.30
TAC(\$)	15.19	16.42	32.02	32.02
E_n(kWh/year)	324.99	353.14	623.45	624.29
Ex_n(kWh/year)	324.99	390.88	692.37	698.75
C_t(\$/kWh)	0.06	0.06	0.06	0.06
$AECP_{el}$(\$)	19.50	21.19	37.41	37.46
$AECP_{ex}$(\$)	19.50	23.45	41.54	41.93
AS_{el}(\$)	4.31	4.77	5.39	5.44
AS_{ex}(\$)	4.31	7.03	9.52	9.91
φ_{CO_2}(ton)	0.65	0.78	1.38	1.40
Z_{CO_2}(\$)	9.42	11.31	20.01	20.30
TAS(\$)	13.73	18.34	29.53	30.21

radiation. Hence, the bifacial unit preferably be at some height (y) to the floor to get radiation on the entire face of the bottom PV panel. The height of the bottom end of the calculation is given as:

$$y = \frac{h}{2Sin\theta} - hSin\theta, \tag{6.33}$$

and the length (Q*B*) of land required to install a bifacial PV/PCM unit is:

$$Q^*B^* = tSin\theta + ytan\theta + \frac{h}{Cos\theta} \tag{6.34}$$

whereas length (Q*F*) required for simple PV/PCM unit is:

$$Q^*F^* = tSin\theta + ytan\theta + \frac{h}{2Cos\theta} \tag{6.35}$$

For the current case, inclination angle (θ) is considered as 25°. Figures 6.14 (a) and 6.14 (b) compares the power output density (power output per unit land/floor/roof area) and energy utilization density (energy utilization per unit land/floor/roof area) of bifacial PV/PCM unit to simple PV/PCM unit and conventional PV system unit respectively. It can be seen from the results that the power output density for the BIF-PV/PCM (V_L/V_R = 16/14) unit is 1.21 times that of the conventional PV system and 1.11 times that of the conventional BIF-PV system. The total energy utilization density of the BIF-PV/PCM system (V_L/V_R = 16/14) is 7.39 times the conventional PV system, 6.89 times the BIF-PV system, and 1.2 times of L_{30} PV/PCM system. The bifacial PV/PCM unit is more beneficial when attached to the buildings as it will reduce the cooling load

of the building by reflecting the incoming radiation. It also has stored heat that can be utilized at nighttime by making some heat discharge arrangements to the PCM region. Various other concentrating type reflectors can be used instead of L shape mirror system to further enhance the system's performance.

Economic, exergoeconomic, and enviroeconomic analysis:

The cost assessment of the system predicts the viability of any system. The main goal of cost assessment is to produce maximum power at minimal investment. The cost assessment can be performed by using the steps shown in Table 6.3[69]:

The economic, exergoeconomic and enviroeconomic analysis for all studied configurations is shown in Table 6.4. An annual interest rate of 4% is assumed on capital investment for a speculated life span of 20 years for all systems. The conventional PV system exhibit a saving of 4.31$ per year from single PV panel of unit area. However, PV/PCM systems, and bifacial PV/PCM system exhibits more savings due to extra electricity production. The $L_{30}PV/PCM$ system exhibit a saving of 4.77$ (per year) while L_{30} BIF-PV/PCM system and BIF-PV/PCM(V_L/V_R = 16/14) system exhibit saving of 5.39$ and 5.44$ respectively for electricity production. Apart from that, the mono-facial and bifacial PV/PCM systems have an advantage of thermal exergy production. Hence, the saving increases to 7.03$, 9.52$, and 9.91$ for L_{30} PV/PCM system, L_{30} BIF-PV/PCM system, and BIF-PV/PCM (V_L/V_R = 16/14) system respectively. Increase in power production from renewable sources like PV technology will benefit us by providing less polluted environment by low carbon emission. This low emission will also benefit us by earning carbon credits and the savings boost further virtually. The total annual saving boosts to 13.73$, 18.34$, 29.53$, and 30.21$ for PV system, L_{30} PV/PCM system, L_{30} BIF-PV/PCM system, and BIF-PV/PCM (V_L/V_R = 16/14) system respectively. The value of tariff for domestic electricity consumption is considered here, while for commercial consumption of electricity are much higher. Hence, the annual savings can increase further for the electricity production in commercial enterprises. Among the studied configurations, the proposed BIF-PV/PCM system (V_L/V_R = 16/14) seems to be most economic. Therefore, the proposed BIF-PV/PCM system (V_L/V_R = 16/14) is considered the most feasible option among all studied configurations.

6.4 Conclusions

In this chapter, a new bifacial PV/PCM technique has been proposed with the help of an experimentally calibrated computational model. In this technique, two PV panels are used with a sandwiched thermal energy storage PCM enclosure (bifurcated type) between the panels. The enhancement in thermo-electric performance is obtained by using proper thermal management and insolation management strategies. Insolation management strategies include an L-shape reflector system which avails the bypassing radiation to the bottom PV panel. However, thermal management strategies include lowering the PV panel temperature with a proper char-

acterization of melting by changing the shape and design of the enclosure. The shape and ratio of the volume bifurcated system are chosen according to melting front morphology, incident radiation, and reflected radiation after many design iterations. Melting behavior, absolutely absorbed energy, electric power output, exergy efficiency, and overall system efficiency are reported in detail. Some essential outcomes are as follows:

1. The new bifacial PV/PCM system exhibit 10.98% and 105% more melting than L_{30} BIF-PV/PCM system and L_{30} PV/PCM system respectively due to more prolonged quasiconvection regime (105 minutes).

2. Electric power output is 77% more in modified BIF-PV/PCM system thanL_{30} PV/PCM due to additional reflected radiation to bottom PV panel and better thermal management of PV panels.

3. The modified BIF-PV/PCM system exhibit high energy utilization efficiency of 73.71%, which is just 10.69%, 10.84%, and 68.74% in conventional BIF-PV, PV, and PV/PCM system respectively.

4. The new bifacial PV/PCM system exhibit 1.21 times power output density and 7.39 times total energy utilization density compared to the conventional PV system.

5. The modified BIF-PV/PCM system exhibit an enhancement of 2.57% in exergy efficiency compared to conventional PV system and seems to be most economical in both electricity and exergy production.

Hence, the modified BIF-PV/PCM system with a bifurcated thermal storage design is recommended due to better thermo-electric performance and waste heat management performance compared to all other configurations. This research would help the research community develop an energy-efficient BIF-PV/PCM system with rectangular and non-rectangular PCM enclosures. The ever-rising energy demands of the world can be minimized by producing extra electric power and storing extra heat passively in more efficient BIF-PV/PCM systems with approximately lesser space requirements.